WRF Wind Power Forecasting in the Coast Ranges of Central California

Kevin T. Clifford

Dept. of Meteorology and Climate Science
San José State University
San Jose, CA

May 12, 2011

Outline

- Background
- Wind Power Forecast Modeling
- Model Setup and Experimental Design
- Results
- Summary and Conclusions

Background: The State of Wind Power

- U.S. grid-connected wind power capacity has increased tenfold since the 1980s (Wiser and Bolinger 2008)
- Increases due in part to wind power production within complex terrain (Gazzilli et al. 2001)
- Before wind power can be integrated into the power network, accurate estimates of its potential contribution are necessary to ensure efficient utilization (Brown et al. 1984)
- Accurate atmospheric modeling within complex terrain is essential for forecasting wind power production but still remains a challenge.

Background: California Coast Ranges

- California Coast Ranges
  - Up to 1.3 km in elevation above mean sea level
  - Parallel to California coastline
  - Topographic barrier separating the Pacific Ocean from California's Central Valley

- Late-spring through mid-fall (LSMF) synoptic conditions ideal for wind power production
  - Eastern Pacific surface high pressure vs. Central Valley / Great Basin thermal low pressure
  - Pressure gradient results in onshore flow of stable marine air
  - Sea breeze and **mountain circulations** couple to enhance near-surface wind speeds

(Fosberg and Schroeder 1966; Burk and Thompson 1996; Zaremba and Carroll 1999; Archer and Jacobson 2005)

Background: Mountain Atmospheric Circulations

- Coast Range LSMF synoptic drivers that lead to increased wind speeds at mountain ridge crest and lee side slopes:
  - Vertical compression of atmosphere (Barry 1992)
  - Gap flow acceleration (Doran and Zhong 2000; Jaramillo and Borja 2004; Sharp and Mass 2004)
  - Gravity wave formation (Doyle and Smith 2003; Zangl 2003)
  - The combination of all three leads to the highest sustained wind speeds (Zangl 2003; Gabersek and Durran 2004; Gabersek and Durran 2006)

The whole is greater than the sum of its parts

Outline

- Background
- **Wind Power Forecast Modeling**
  - Calculating wind power
  - The WRF model
- Model Setup and Experimental Design
- Results
- Summary and Conclusions

Wind Power Forecast Modeling: Calculating Wind Power

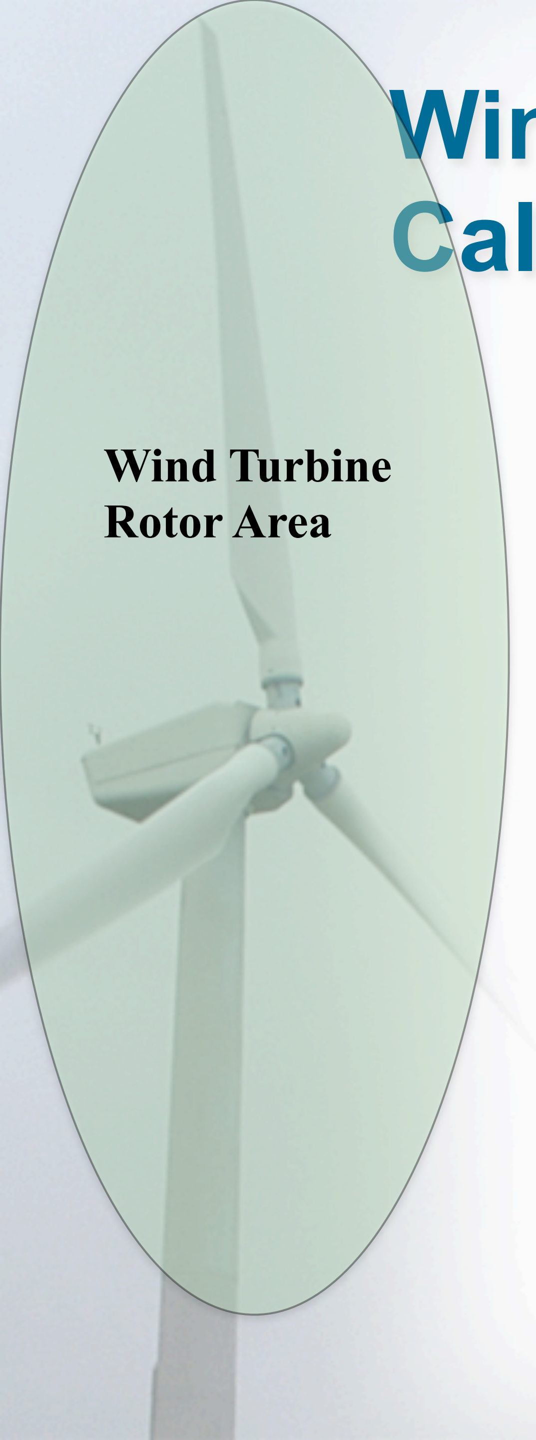

Wind Power (Watts)

$$P = \frac{1}{2}\rho A U^3$$

ρ = Air Density (kg m^{-3})

A = Rotor Area (m^2)

U = Rotor Area Mean Wind Speed (m s^{-1})

How is the rotor area mean wind speed determined?

Calculating Wind Power: Determining *U*

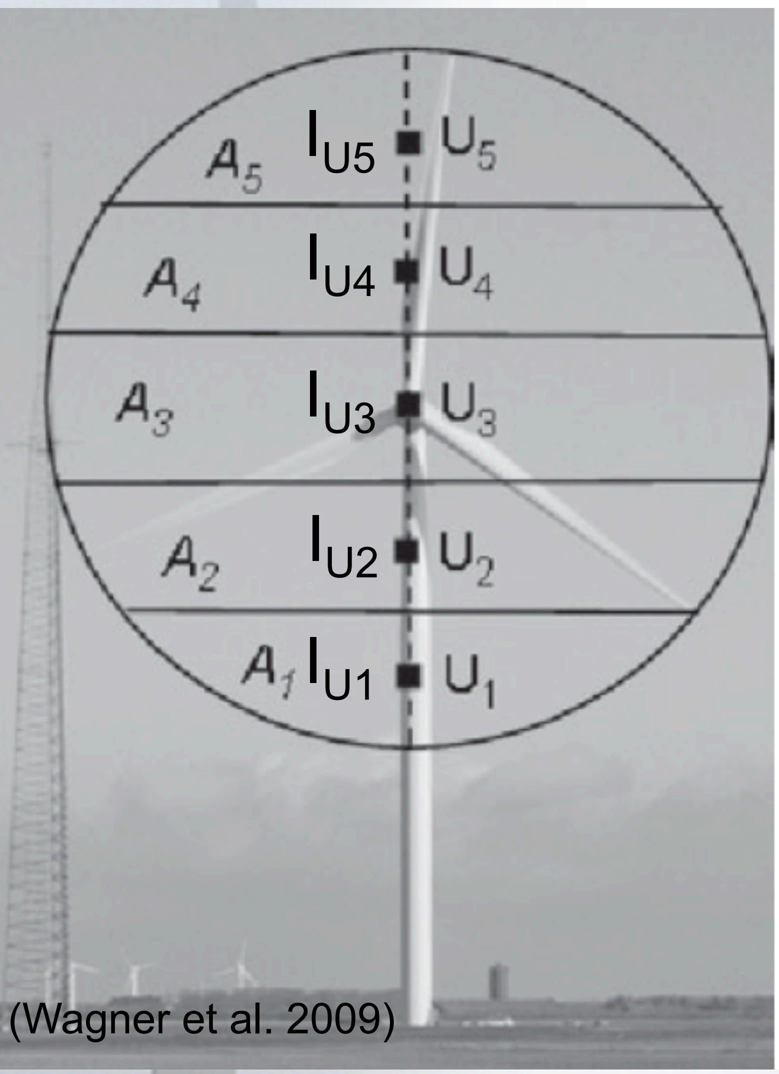

(Wagner et al. 2009)

- Horizontal Turbulence Intensity (unitless)

$$I_U = \frac{\sigma_U}{U(z)}$$

- True Flux Wind Speed (m s^{-1})

$$U_I = \sqrt[3]{U(z)^3(1+3I_U{}^2)}$$

- Equivalent Wind Speed (m s^{-1})

$$U_{equiv} = \frac{2}{A}\int_{H-r}^{H+r} U_I(r^2 - H^2 + 2Hz - z^2)^{1/2}\,dz$$

(Wagner et al. 2009; Wharton and Lundquist 2010)

Wind Power Forecast Modeling: Calculating Wind Power

- Wind turbines maximize power production at their **turbine power rating** (P_R)

- **Capacity Factor** (*CF*) measures the ratio of actual to optimal performance

$$CF = \frac{P}{P_R} = \frac{\frac{1}{2}\rho A (U_{equiv})^3}{P_R}$$

- Typically, modern wind turbines have an annual CF of 35 to 48 percent (Wiser and Bolinger 2009).

The Weather Research and Forecasting Model (WRF)

- Community supported mesoscale model developed by NCAR/NCEP (Skamarock et al. 2010)
  - Eulerian mass dynamics
  - Full suite of physics
- All aspects of WRF are user specified
  - Time step of prognostic equations
  - Physics and Dynamics Parameterizations
- High temporal and spatial resolution modeling using domain nesting
- Better suited for resolving the near surface atmospheric conditions in complex terrain (Rife et al. 2004; Zagar et al. 2006; Jimenez et al. 2010)

The Weather Research and Forecasting Model (WRF)

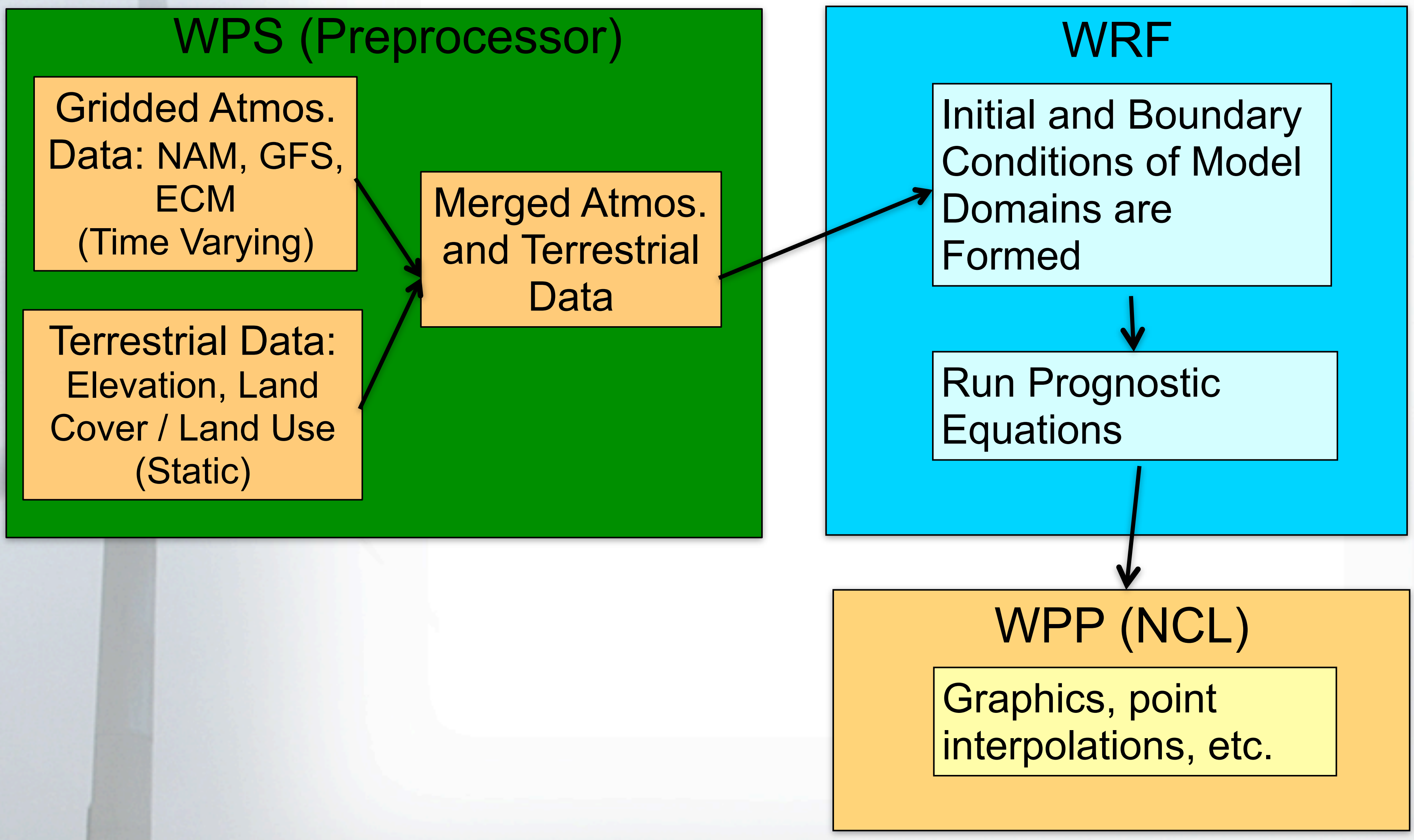

Outline

- Background
- Wind Power Forecast Modeling
- **Model Setup and Experimental Design**
  - Goals
  - WRF Model Configuration
  - Observational Data
  - Statistical Comparisons
- Results
- Summary and Conclusions

Goals

During LSMF synoptic conditions:

1. Simulate the near-surface winds in Coast Ranges
2. Simulate winds and wind power in Altamont Pass
3. Assess the accuracy and potential of WRF as a wind power forecasting tool

WRF Model Configuration: Domains

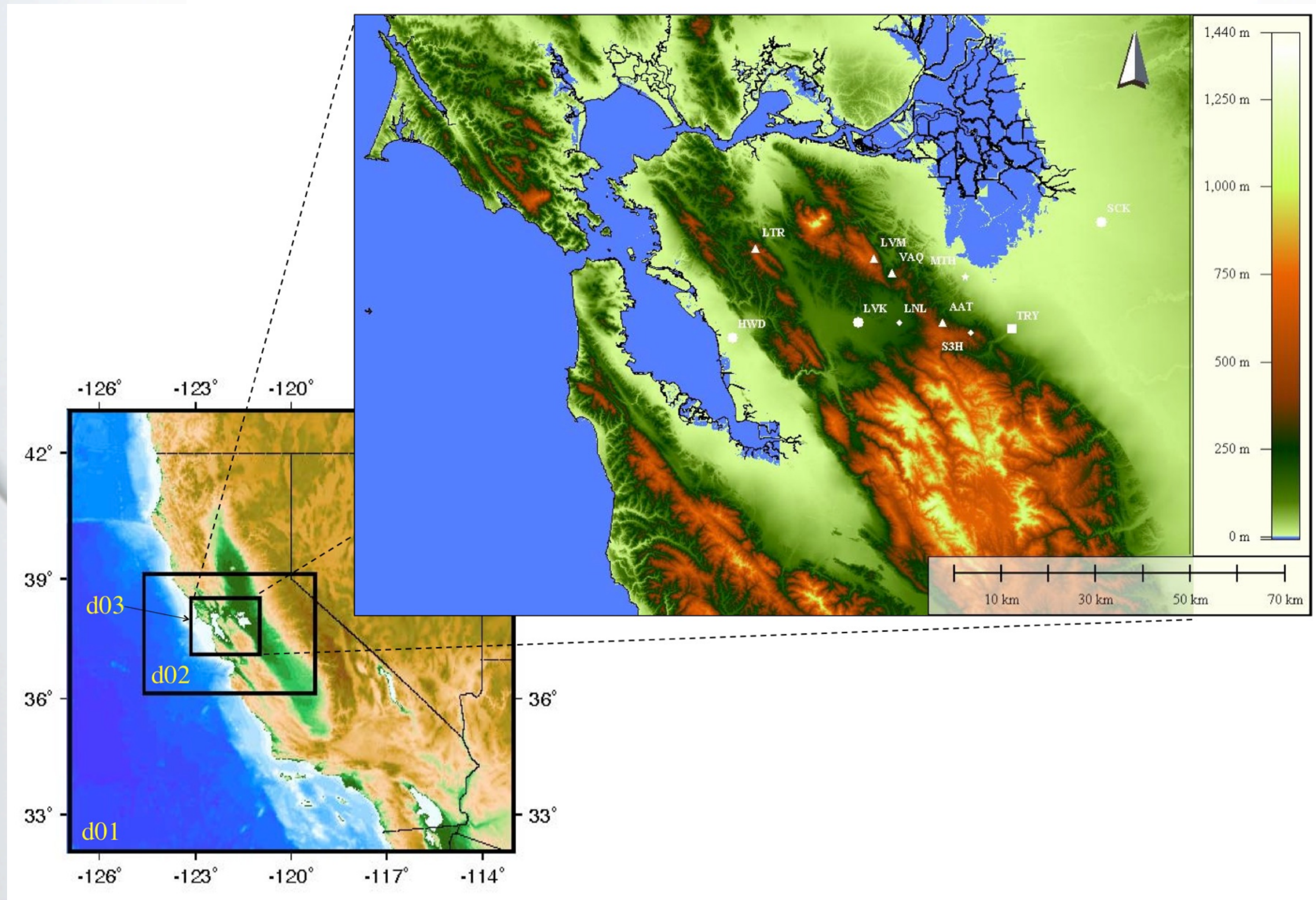

Spatial configuration of domains for WRF simulation: three domains two-way nested with 9, 3, and 1 km resolution.

WRF Model Configuration: Domains

- Horizontal Resolution:
  - California – 9 km
  - Central California – 3 km
  - San Francisco Bay Area – 1 km
- Vertical Resolution:
  - 52 terrain-following hydrostatic pressure levels
  - Top Level: 50 hPa
  - 18 levels below 300 m AGL

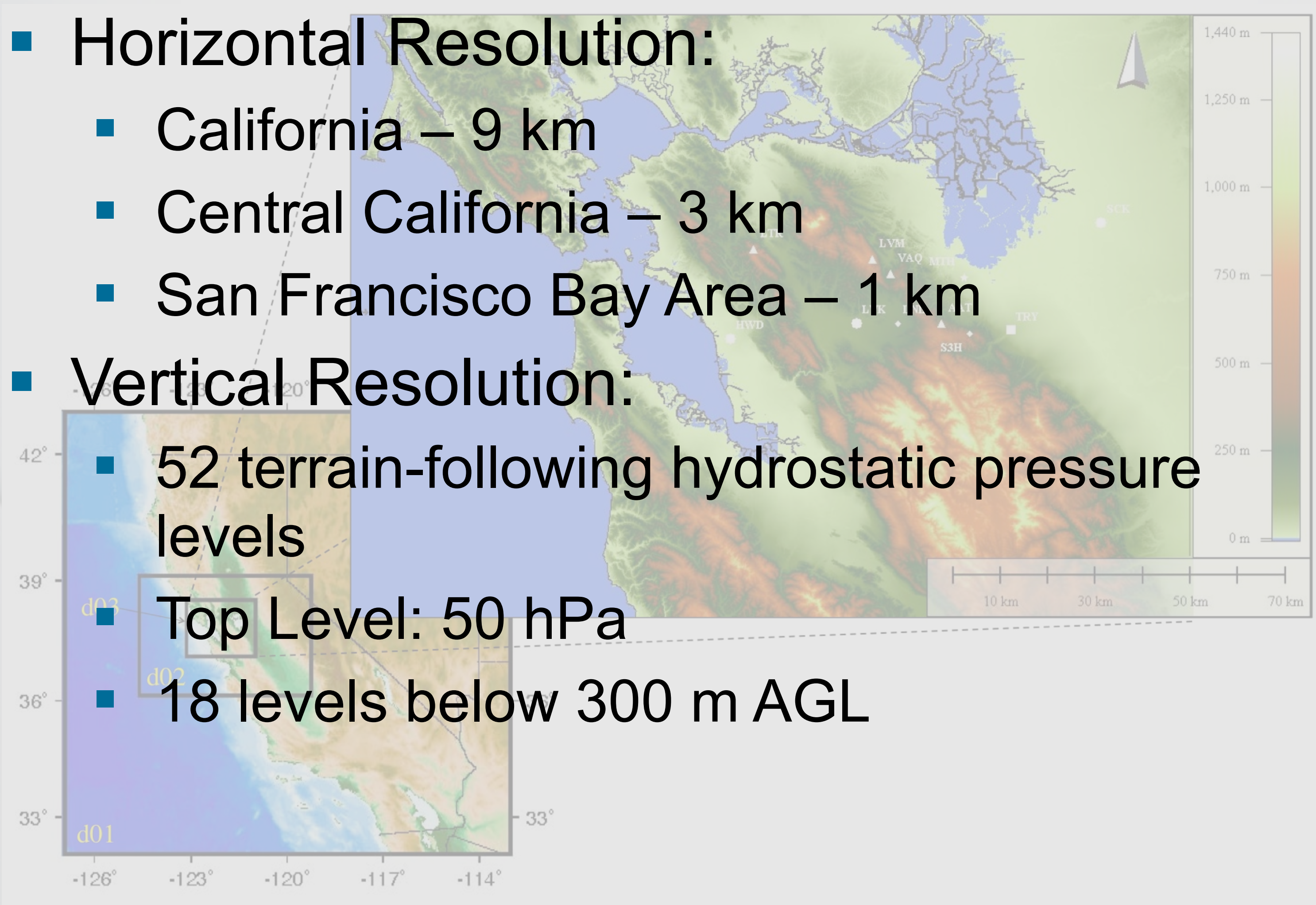

WRF Model Configuration: Case Model Runs

- Five 84-hour case model runs

Case	Beginning Date	Ending Date
1	0000 UTC July 6 2010	1200 UTC July 9 2010
2	0000 UTC July 18 2010	1200 UTC July 21 2010
3	0000 UTC July 24 2010	1200 UTC July 27 2010
4	0000 UTC July 29 2010	1200 UTC August 1 2010
5	0000 UTC August 4 2010	1200 UTC August 7 2010

- Near ideal LSMF synoptic conditions
- Initial and boundary conditions were obtained from NAM 218

Observational Data and Comparison Sites

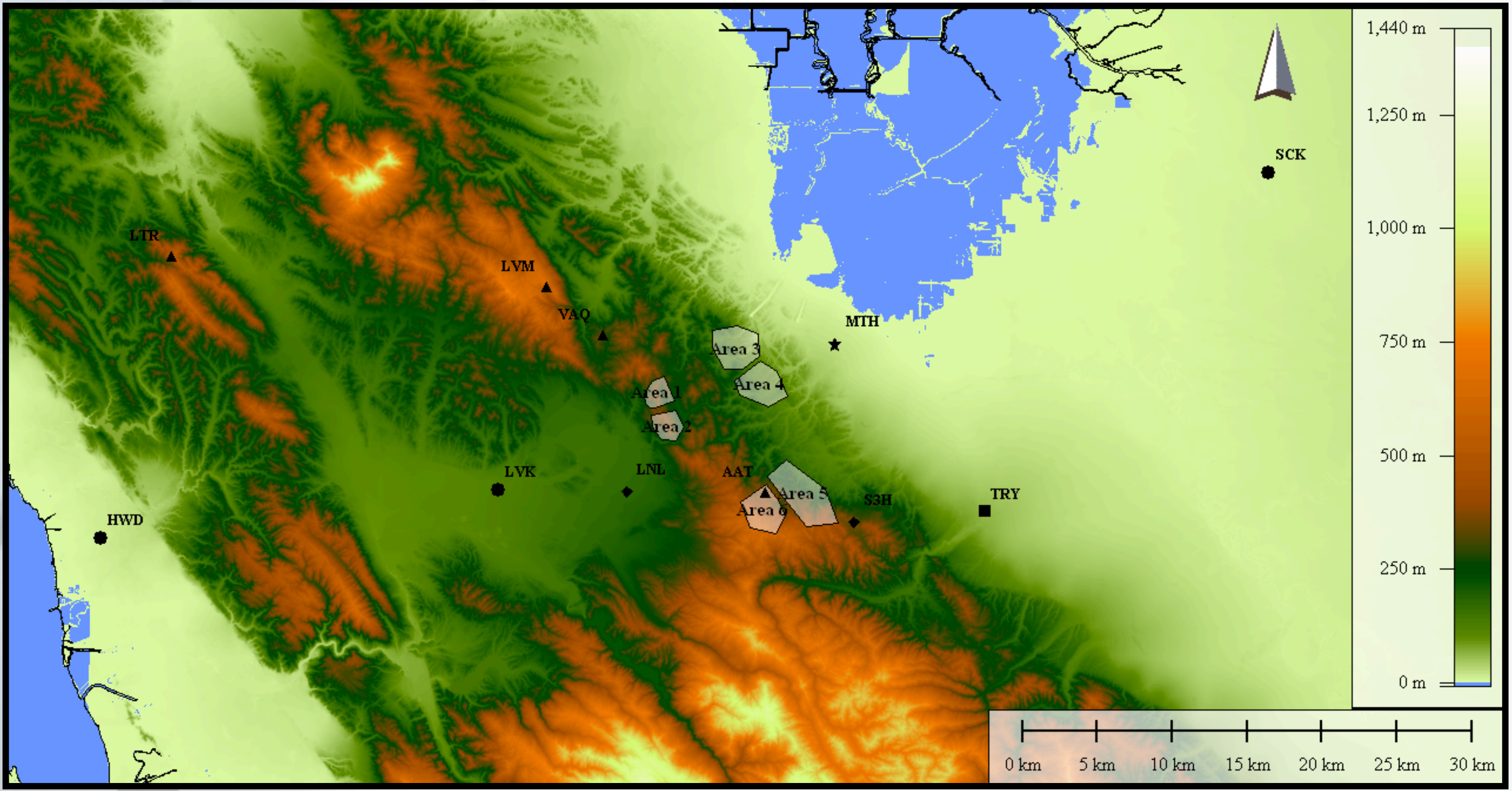

The comparison sites used for WRF evaluation are from the RAWS (triangles), METAR (circles), CARB (squares), CWOP (stars), and LLNL (diamonds) observation networks. The six white blob Areas are comparison regions of the Altamont Pass wind farm.

Modeled and Observed Comparisons

- Wind Direction
- Horizontal Turbulence Intensity
- Daily Wind Power Production

Wind Speed Statistical Comparisons

- **Mean Absolute Error (MAE)**

$$MAE = \frac{1}{n}\sum \left| F - A \right|$$

- **Root Mean Square Error (RMSE)**

$$RMSE = \sqrt{\frac{1}{n}\sum (F - A)^2}$$

- **Anomaly Correlation (ACC)**

$$ACC = \frac{n\sum FA - \sum F \sum A}{\sqrt{\left[n\sum F^2 - \left(\sum F\right)^2\right]\left[n\sum A^2 - \left(\sum A\right)^2\right]}}$$

Wind Speed Statistical Performance

Grade	MAE ($m\ s^{-1}$)	RMSE ($m\ s^{-1}$)	ACC (unitless)
Poor	> 3.0	> 3.0	< 0.50
Acceptable	3.0	3.0	0.50
Good	2.5	2.5	0.60
Excellent	2.0	2.0	0.75

Wind Speed Statistical Comparisons

- Statistical performance was calculated for the whole 84 hour model run as well as individual 24 hour periods

Model Evaluation Periods	Time Period
Day 1	0 to 24
Day 2	24 to 48
Day 3	48 to 72
Day 4	72 to 84
All Days	0 to 84

- Day 1 and Day 2 model accuracy is much more critical in terms of energy planning (Bathurst et al. 2002; Kariniotakis et al. 2004), and their results are highlighted

Outline

- Background
- Wind Power Forecast Modeling
- Model Setup and Experimental Design
- **Results**
  - Coast Range Near-Surface Winds
  - Altamont Pass Winds
  - Altamont Pass Wind Power Modeling
  - Wind Power Modeling Performance
- Summary and Conclusions

a. Coast Range Near-Surface Winds: Wind Speed MAE

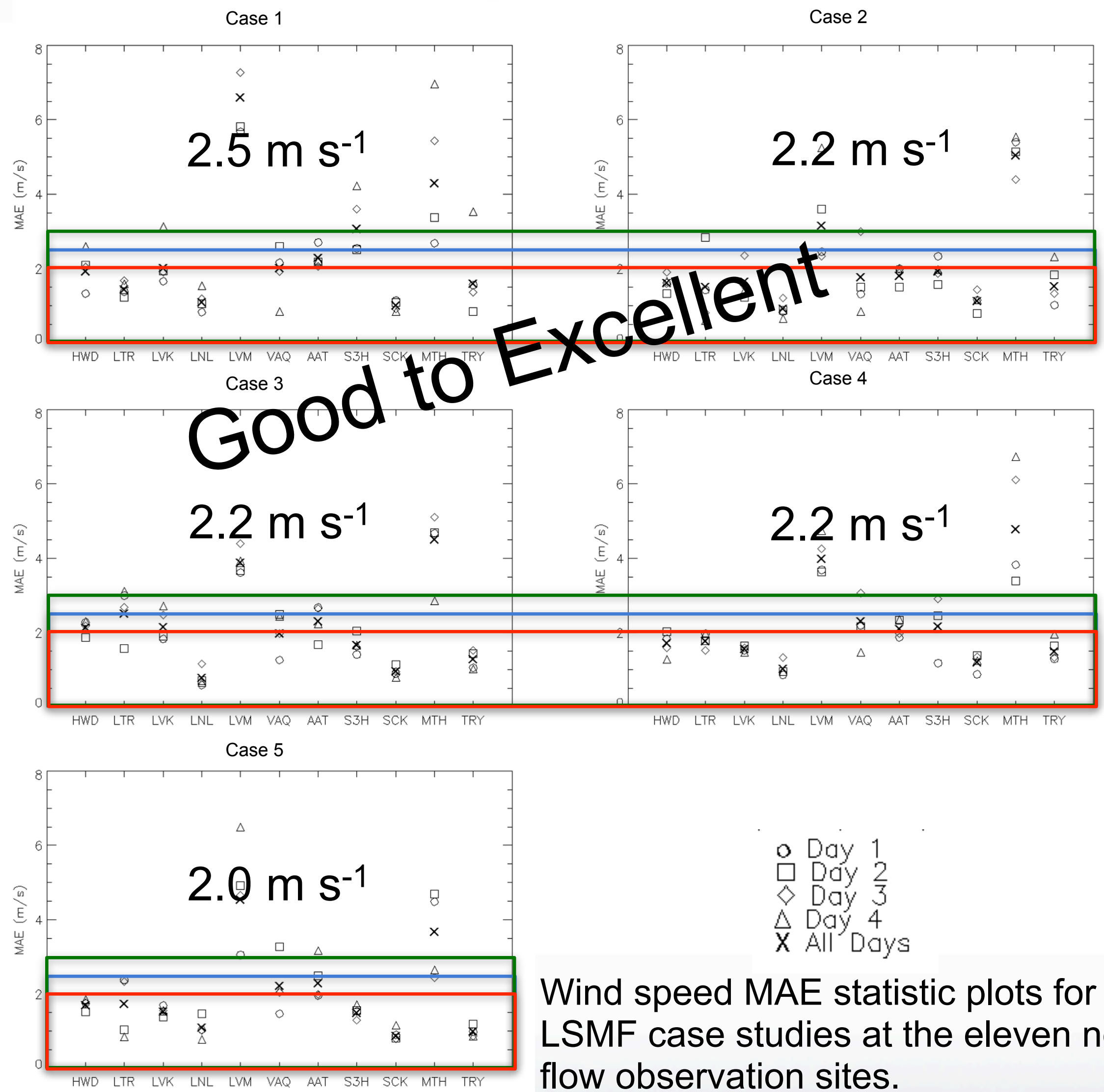

Wind speed MAE statistic plots for the five LSMF case studies at the eleven near-surface flow observation sites.

a. Coast Range Near-Surface Winds: Wind Speed RMSE

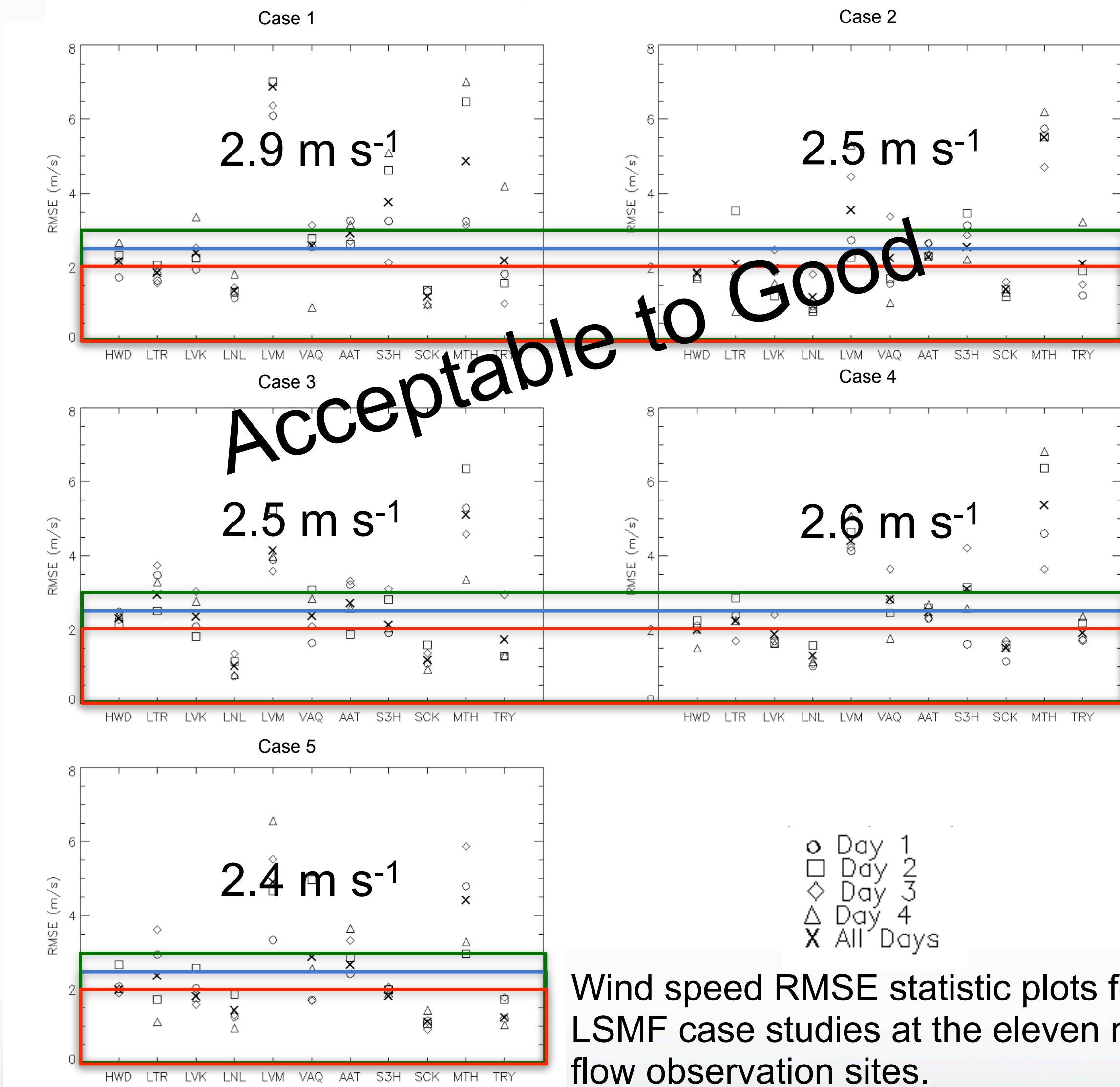

Wind speed RMSE statistic plots for the five LSMF case studies at the eleven near-surface flow observation sites.

a. Coast Range Near-Surface Winds: Wind Speed ACC

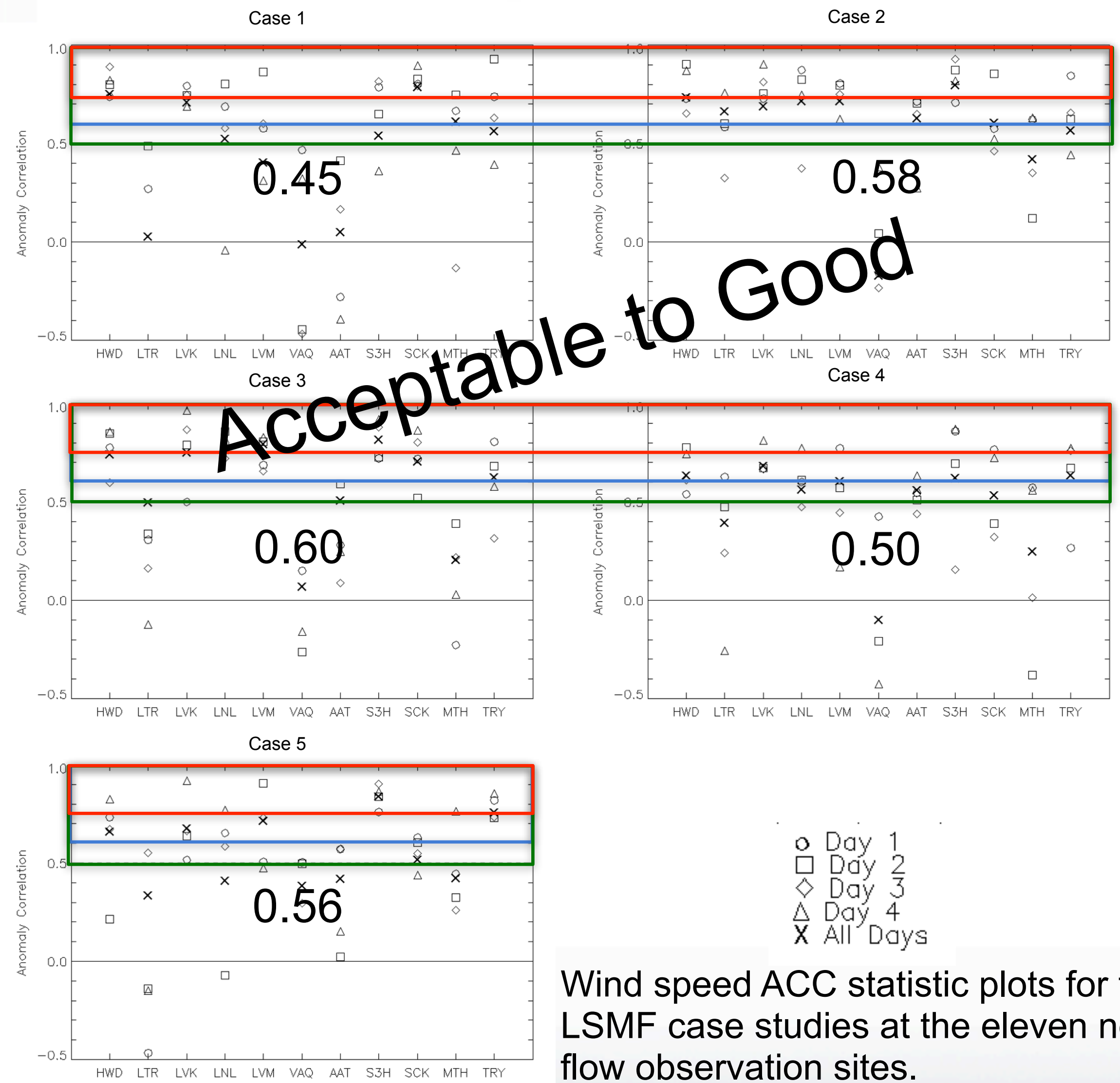

Wind speed ACC statistic plots for the five LSMF case studies at the eleven near-surface flow observation sites.

a. Coast Range Near-Surface Winds: Wind Direction

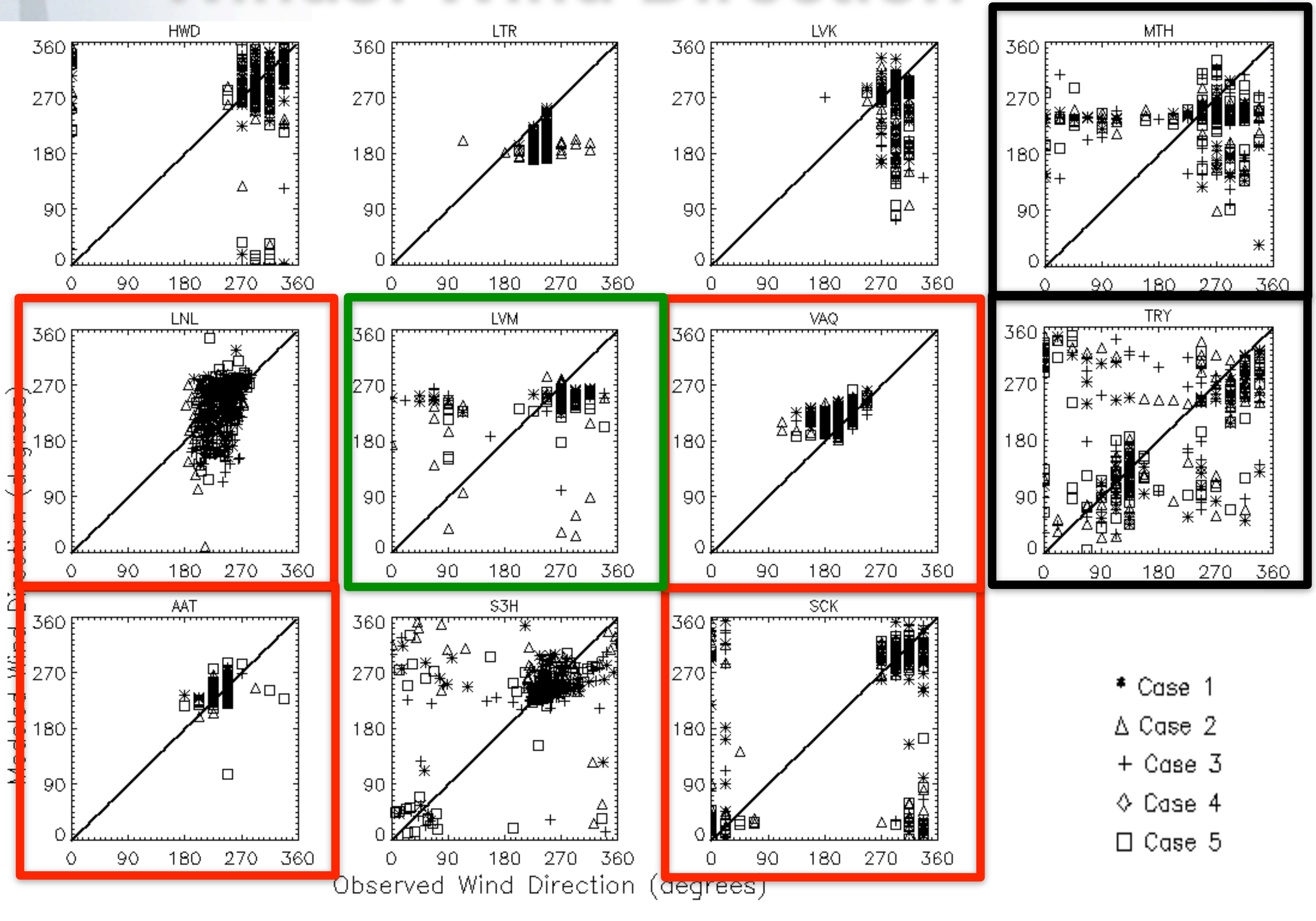

a. Coast Range Near-Surface Winds: Additional Parameters

- In addition to the wind field, several other near-surface atmospheric parameters were tested for these eleven sites
- Over all five cases at all eleven sites:

Atmospheric Parameter	MAE	RMSE	ACC
2 m Temperature	2.0 K	2.5 K	0.70
2 m Relative Humidity	10 %	12 %	0.60
Surface Pressure	2 hPa	2.5 hPa	0.65

- Overall...**Good** to **Excellent** performance

a. Coast Range Near-Surface Winds: Summary

- LNL and SCK
  - Lowest MAEs and RMSEs and highest ACCs
  - Good wind direction agreement
  - **Excellent** model performance
- MTH and LVM
  - Highest MAEs and RMSEs and lowest ACCs
  - Poor to acceptable wind direction agreement
  - **Poor** to **Acceptable** model performance
- AAT and VAQ
  - Average MAE and RMSE
  - Average ACC for AAT and below average ACC for VAQ
  - Good wind direction agreement
  - **Acceptable** to **Good** model performance

b. Altamont Pass Winds: Wind Speed Statistics

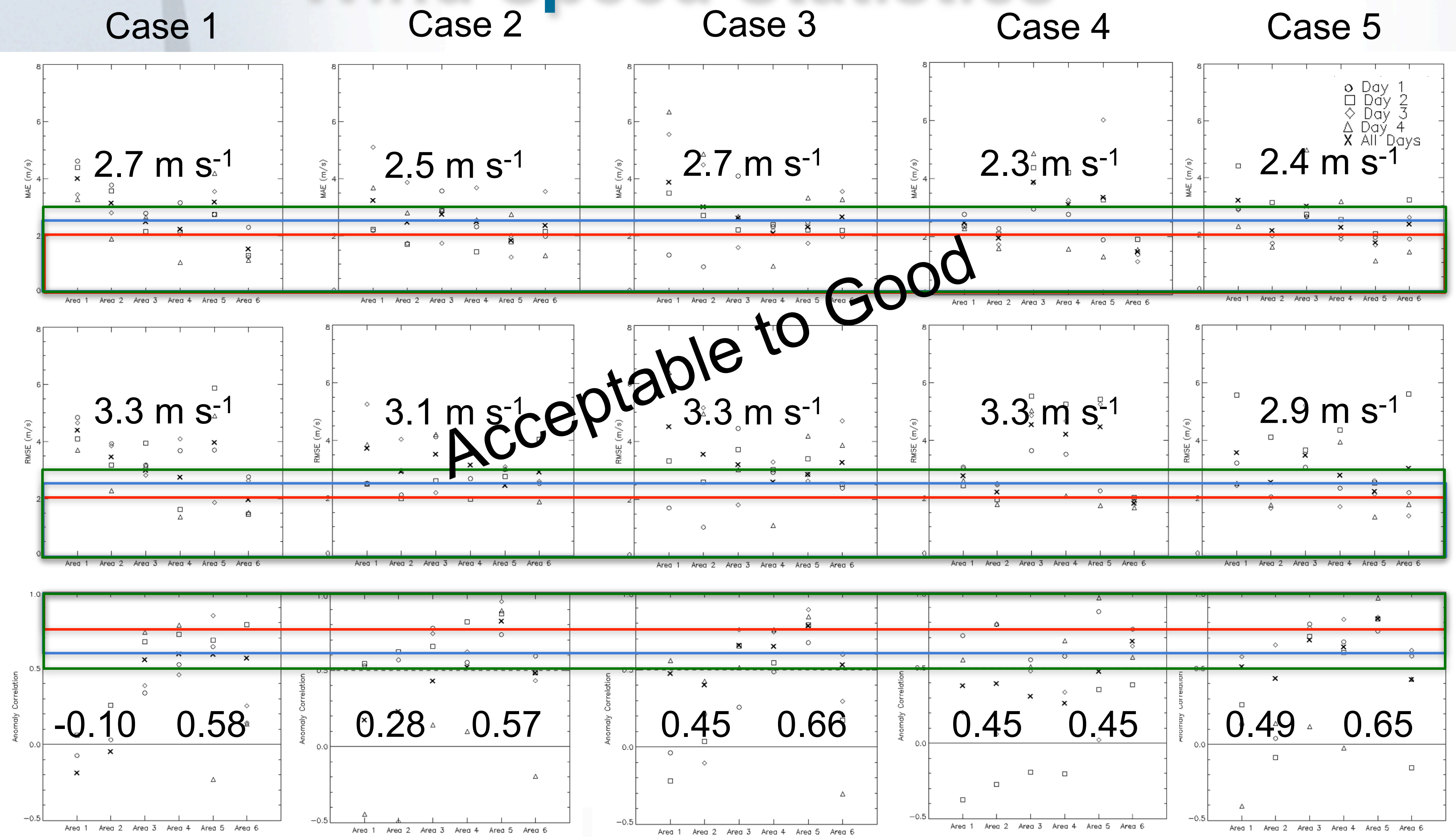

Wind Speed MAE (top row), RMSE (middle row), and ACC (bottom row) statistics for the five LSMF case studies at the six Altamont Pass observation areas.

b. Altamont Pass Winds: Wind Direction

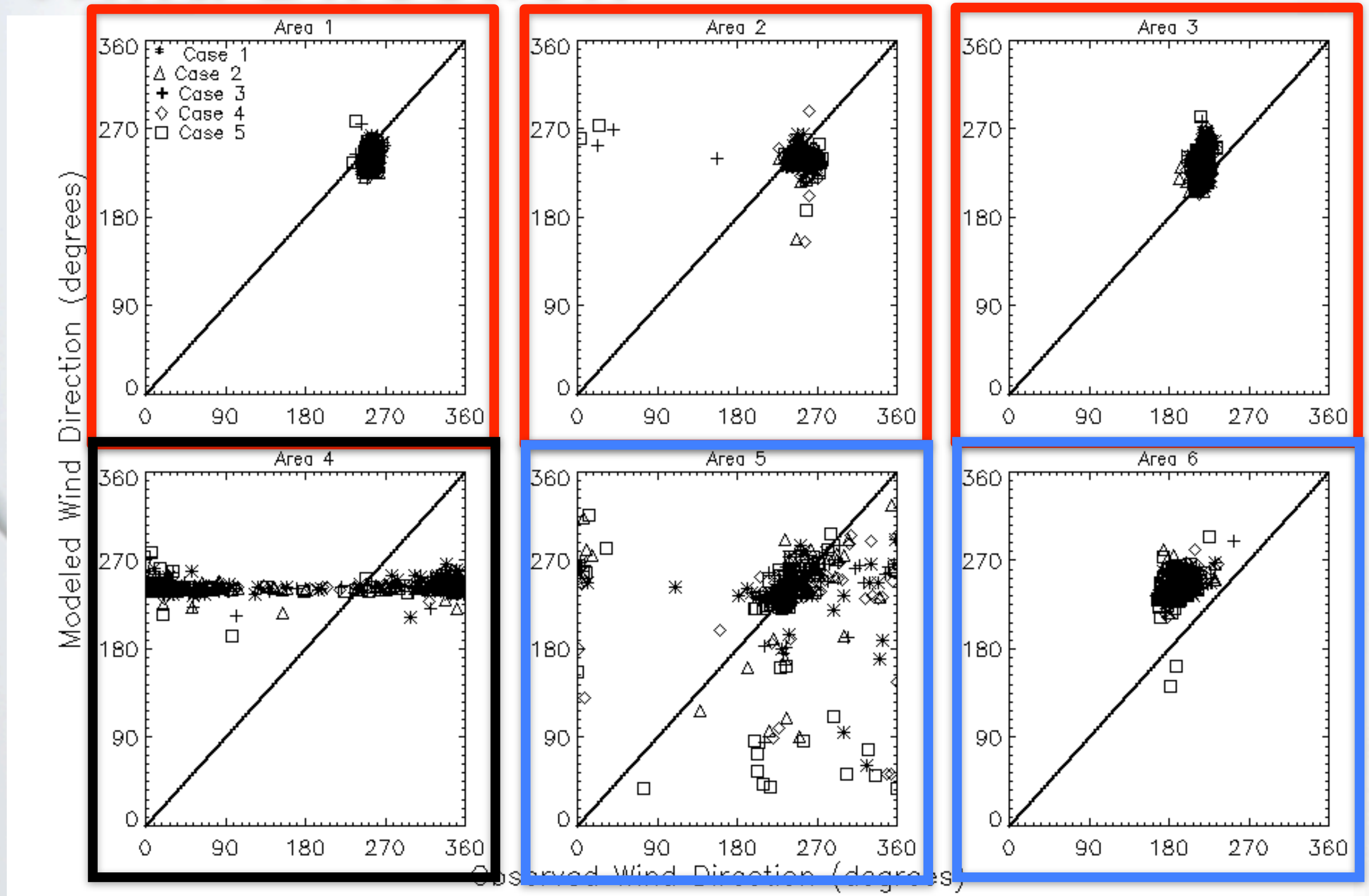

Modeled versus observed wind direction for the five LSMF case studies at the six Altamont Pass observation areas.

b. Altamont Pass Winds: Horizontal Turbulence Intensity

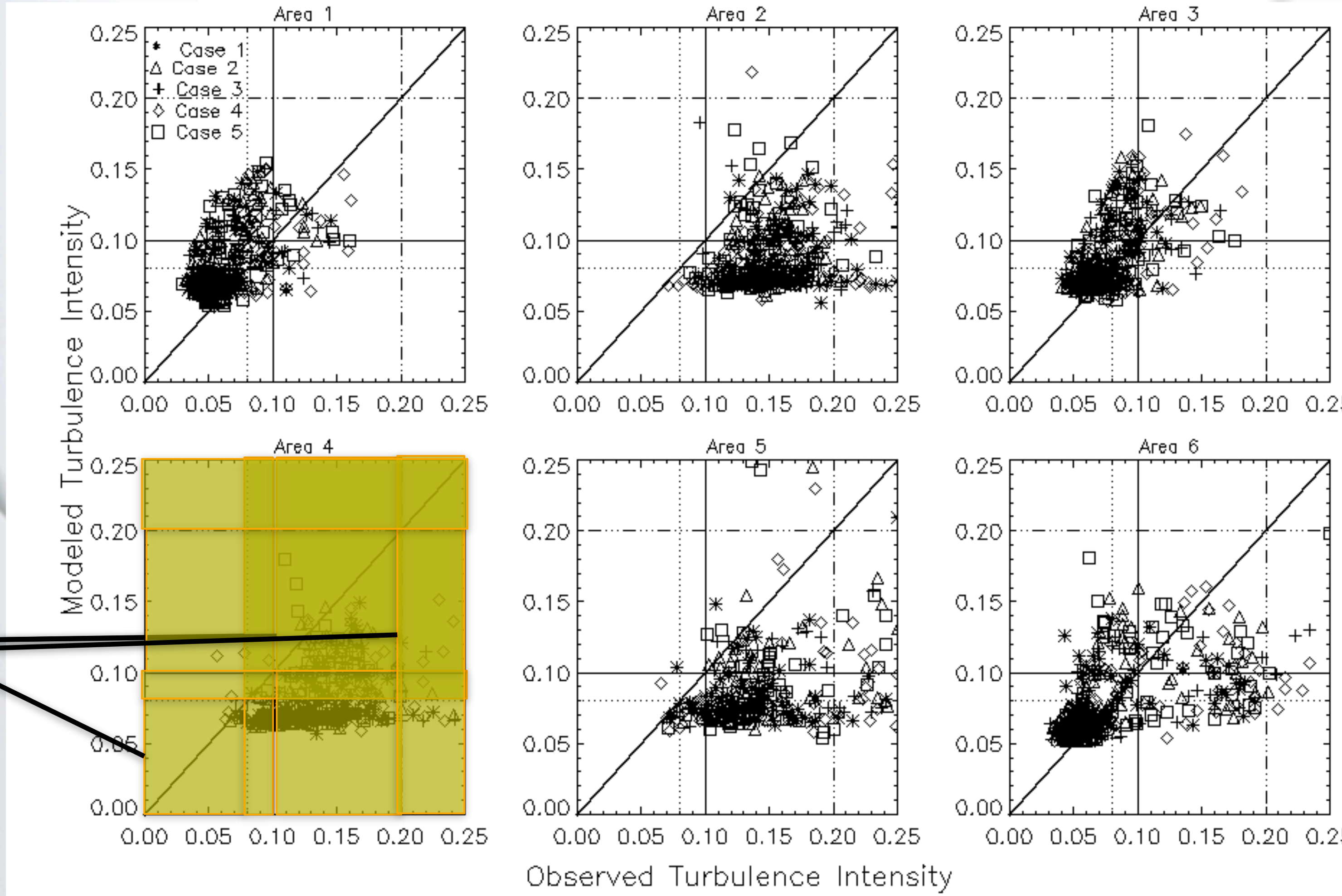

Modeled versus observed turbulence intensity for the five LSMF case studies at the six Altamont Pass observation areas. Horizontal and vertical lines indicate stable (dotted), neutral (solid), and convective (dash-dotted) atmospheric conditions.

b. Altamont Pass Winds: Horizontal Turbulence Intensity

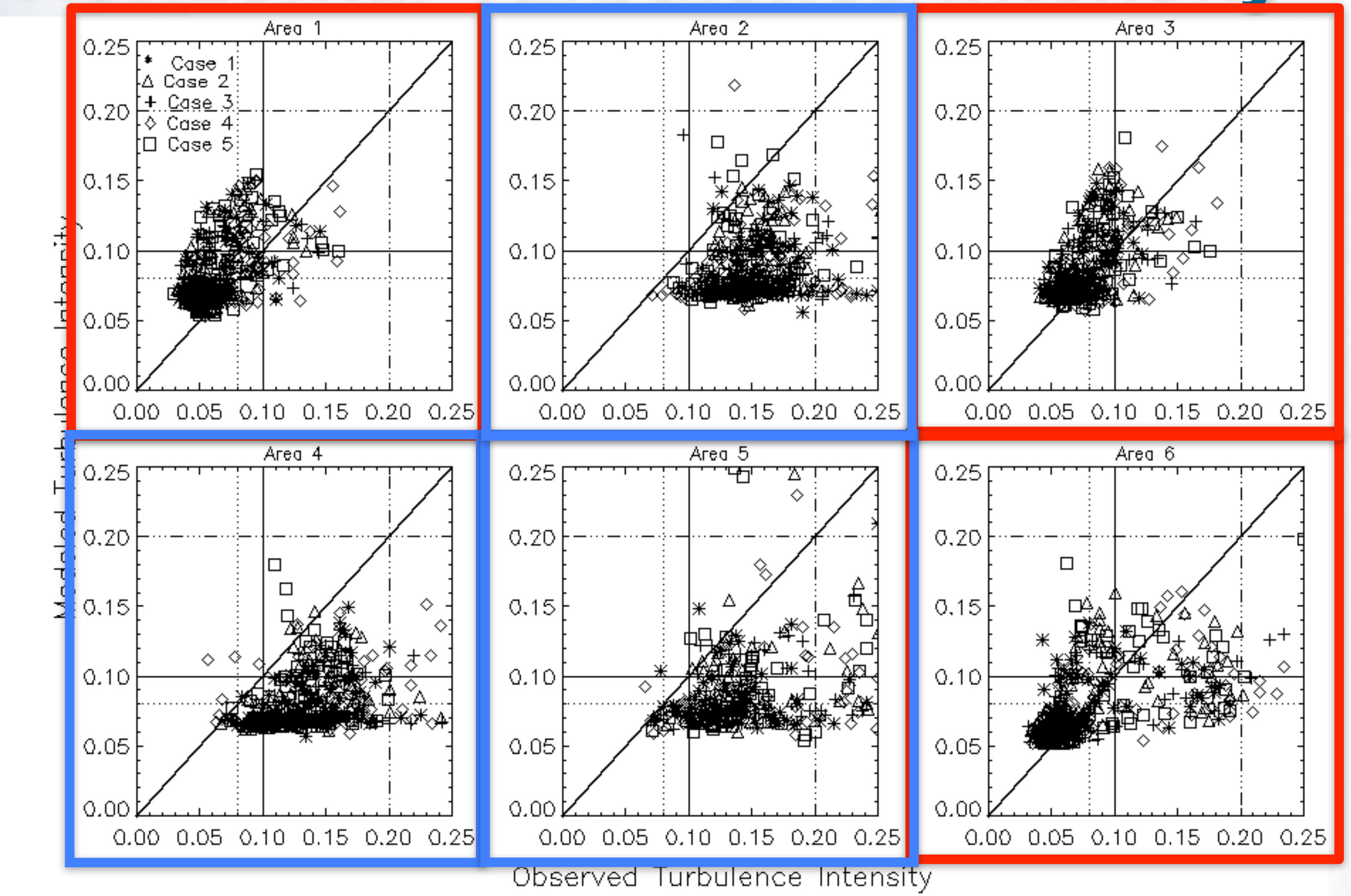

Modeled versus observed turbulence intensity for the five LSMF case studies at the six Altamont Pass observation areas. Horizontal and vertical lines indicate stable (dotted), neutral (solid), and convective (dash-dotted) atmospheric conditions.

b. Altamont Pass Winds: Summary

- Areas 1 and 2
  - **Acceptable** to **Good** MAE and RMSE performance
  - **Poor** ACC performance
  - Good wind direction and I_U agreement
- Area 4
  - **Good** to **Excellent** wind speed statistical performance
  - Good I_U agreement
  - Poor wind direction agreement
- Areas 3, 5, and 6
  - **Good** to **Excellent** wind speed statistical performance
  - Good wind direction and I_U agreement

c. Wind Power Modeling

- WRF-modeled winds and atmospheric stability used to determine rotor area ***equivalent winds (Ue)***
- ***Wind power (P)*** and ***capacity factor (CF)***
- Case 3: typical LSMF 24 hour period
  - Gravity wave conditions were seen, especially during the evening and night hours
  - WRF modeled and observed conditions were in good to excellent agreements (MAE = 2.4 m s^{-1}, RMSE = 2.8 m s^{-1}, and ACC = 0.74)

c. Wind Power Modeling
July 24 1800 UTC (7/24 11 LT)

Equivalent Wind Speeds

CF

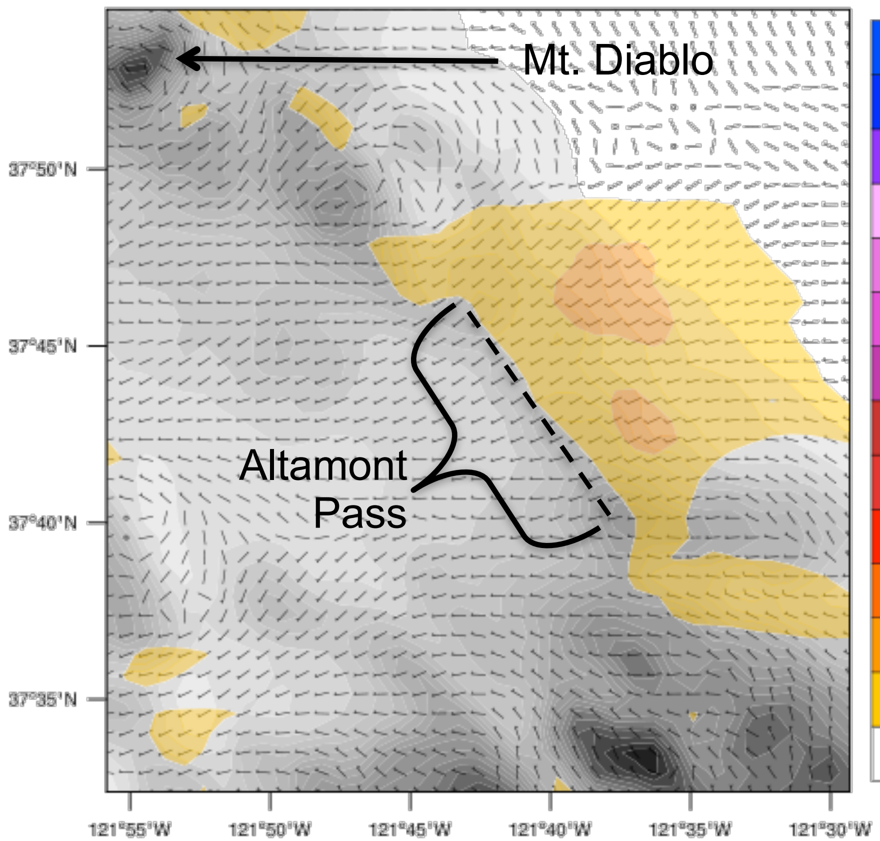

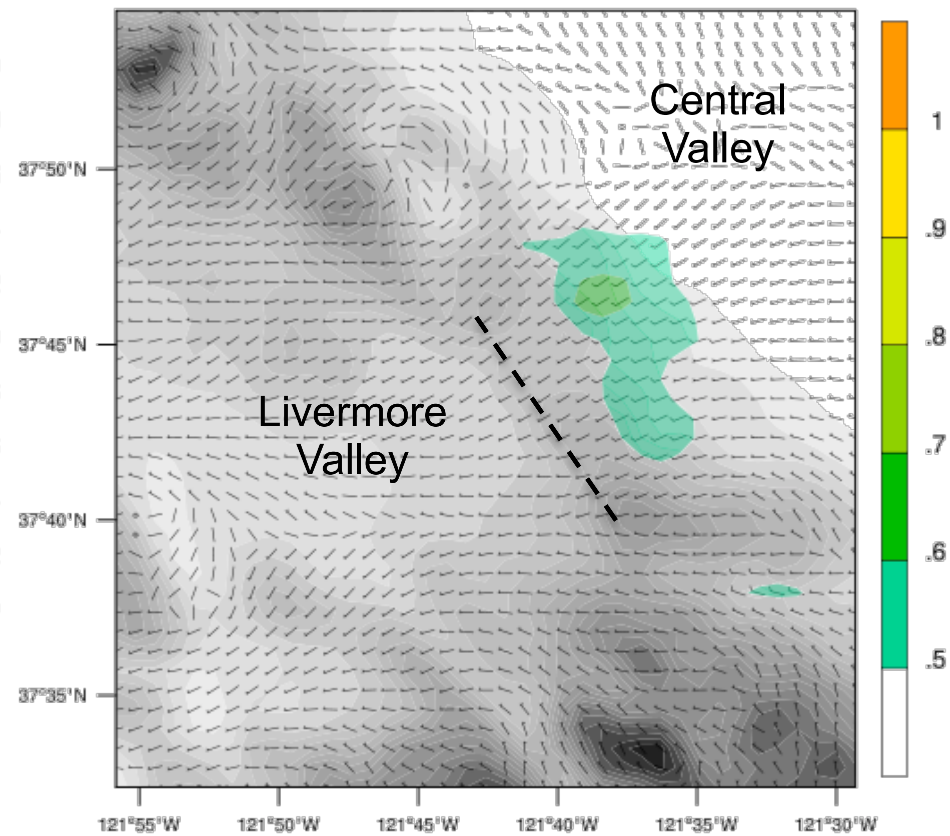

Elevation contoured every 100 m starting at 0 m AMSL (white). (a) Hub-height equivalent winds. Wind barbs, 10 m s^{-1}; half barb, 5 m s^{-1}. Winds ≥ 6 m s^{-1} are shaded in increments of 2 m s^{-1}. (b) Hub-height CF. CFs ≥ 0.5 are shaded in increments of 0.1. Dashed line marks location of Altamont Pass western ridgeline crest.

c. Wind Power Modeling
July 24 1800 UTC (7/24 11 LT)

Light Winds and low CF

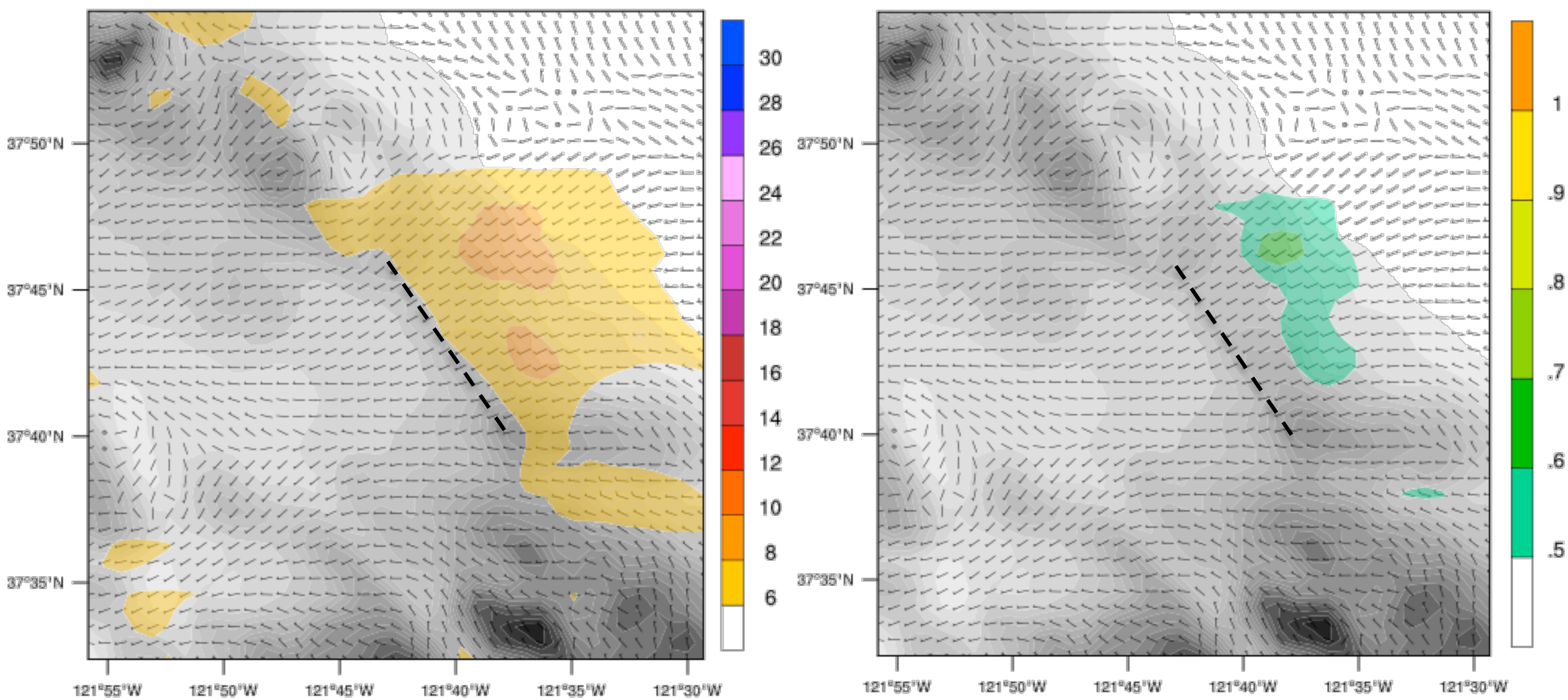

Elevation contoured every 100 m starting at 0 m AMSL (white). (a) Hub-height equivalent winds. Wind barbs, 10 m s^{-1}; half barb, 5 m s^{-1}. Winds $\geq$ 6 m s^{-1} are shaded in increments of 2 m s^{-1}. (b) Hub-height CF. CFs $\geq$ 0.5 are shaded in increments of 0.1. Dashed line marks location of Altamont Pass western ridgeline crest.

c. Wind Power Modeling July 24 2100 UTC (7/24 14 LT)

Winds and CF reach minimum in early afternoon

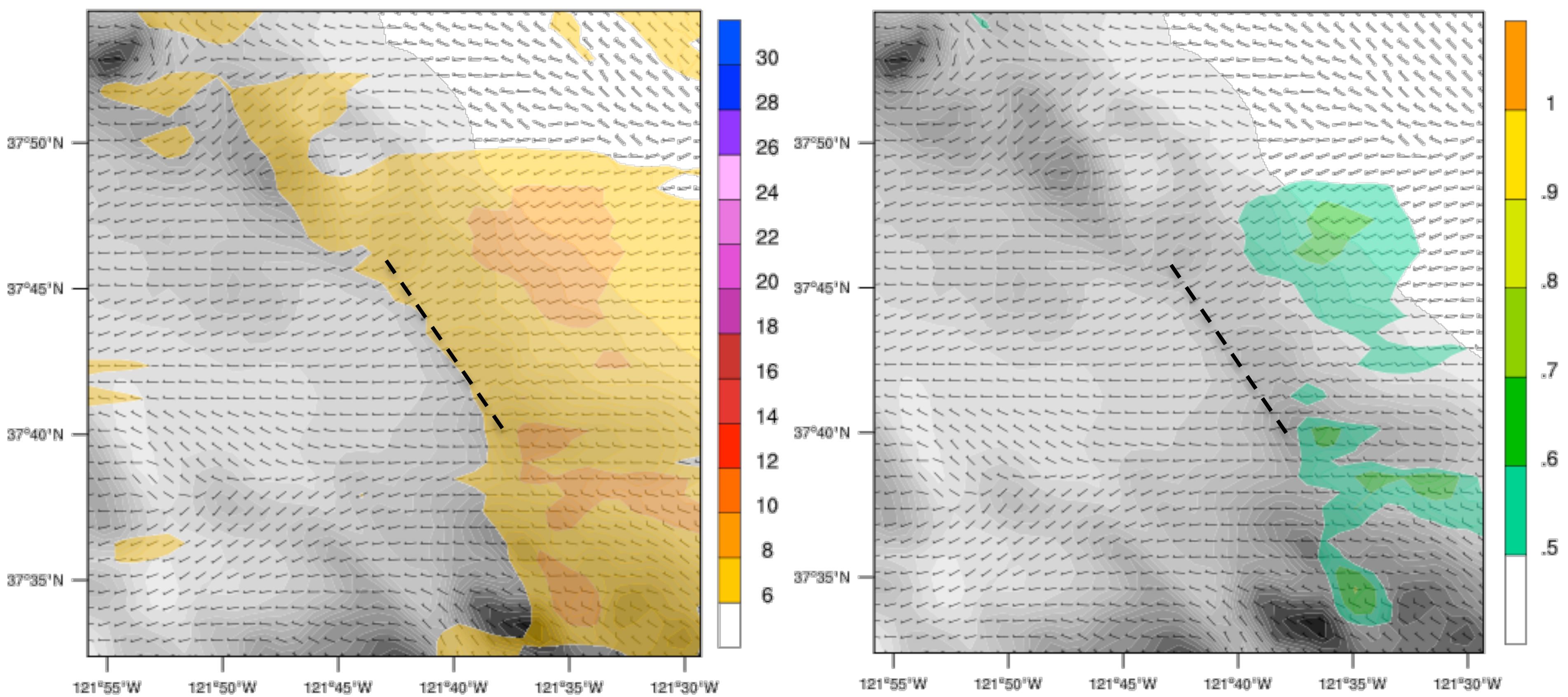

Elevation contoured every 100 m starting at 0 m AMSL (white). (a) Hub-height equivalent winds. Wind barbs, 10 m s^{-1}; half barb, 5 m s^{-1}. Winds $\geq$ 6 m s^{-1} are shaded in increments of 2 m s^{-1}. (b) Hub-height CF. CFs $\geq$ 0.5 are shaded in increments of 0.1. Dashed line marks location of Altamont Pass western ridgeline crest.

c. Wind Power Modeling July 25 0000 UTC (7/24 17 LT)

Winds and CF increase by 2-5 m s^{-1} and 0.2 to 0.3

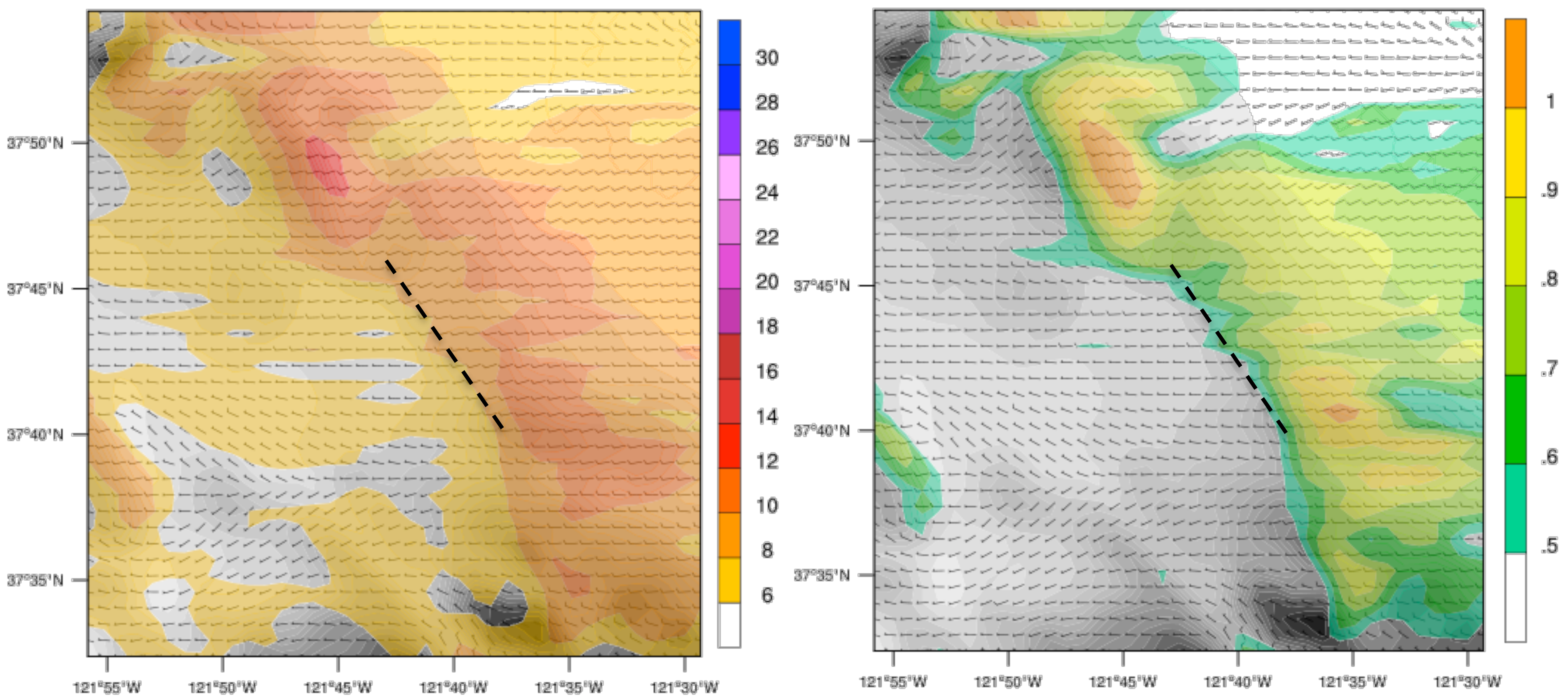

Elevation contoured every 100 m starting at 0 m AMSL (white). (a) Hub-height equivalent winds. Wind barbs, 10 m s^{-1}; half barb, 5 m s^{-1}. Winds $\geq$ 6 m s^{-1} are shaded in increments of 2 m s^{-1}. (b) Hub-height CF. CFs $\geq$ 0.5 are shaded in increments of 0.1. Dashed line marks location of Altamont Pass western ridgeline crest.

c. Wind Power Modeling July 25 0300 UTC (7/24 20 LT)

Wind increases an additional 4-6 m s^{-1} and CF of >0.9

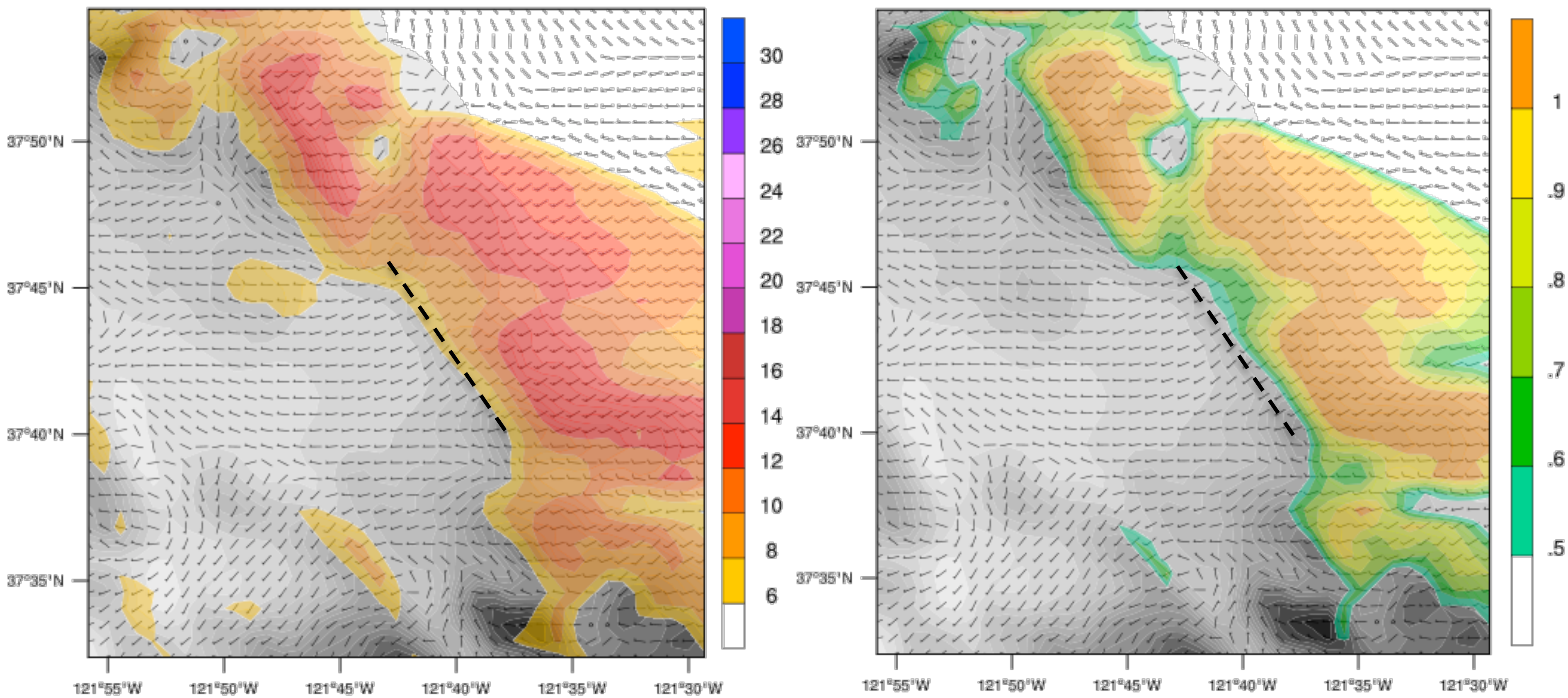

Elevation contoured every 100 m starting at 0 m AMSL (white). (a) Hub-height equivalent winds. Wind barbs, 10 m s^{-1}; half barb, 5 m s^{-1}. Winds $\geq$ 6 m s^{-1} are shaded in increments of 2 m s^{-1}. (b) Hub-height CF. CFs $\geq$ 0.5 are shaded in increments of 0.1. Dashed line marks location of Altamont Pass western ridgeline crest.

c. Wind Power Modeling July 25 0600 UTC (7/24 23 LT)

Further wind and CF increases… near peak values

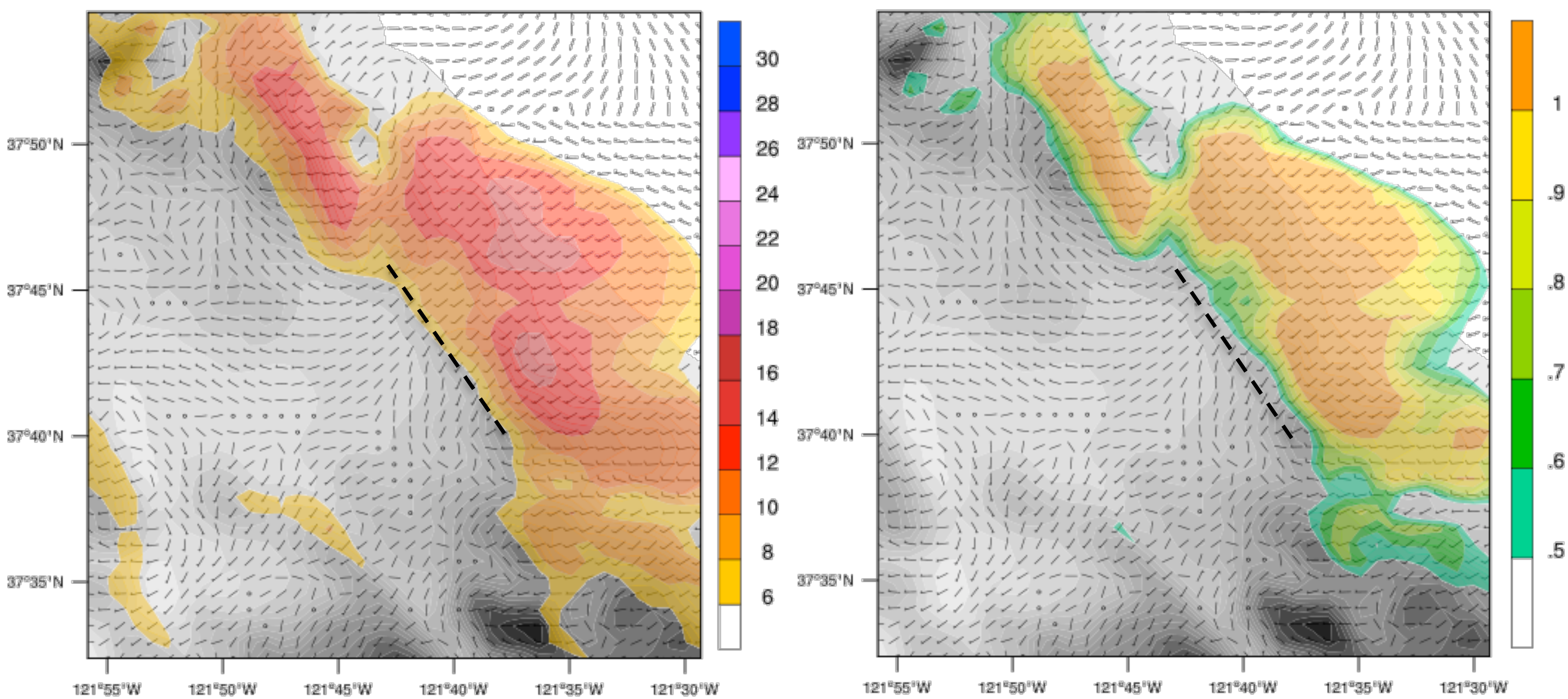

Elevation contoured every 100 m starting at 0 m AMSL (white). (a) Hub-height equivalent winds. Wind barbs, 10 m s^{-1}; half barb, 5 m s^{-1}. Winds $\geq$ 6 m s^{-1} are shaded in increments of 2 m s^{-1}. (b) Hub-height CF. CFs $\geq$ 0.5 are shaded in increments of 0.1. Dashed line marks location of Altamont Pass western ridgeline crest.

c. Wind Power Modeling July 25 0900 UTC (7/25 02 LT)

Winds and CF decrease back down to 2000 LT levels

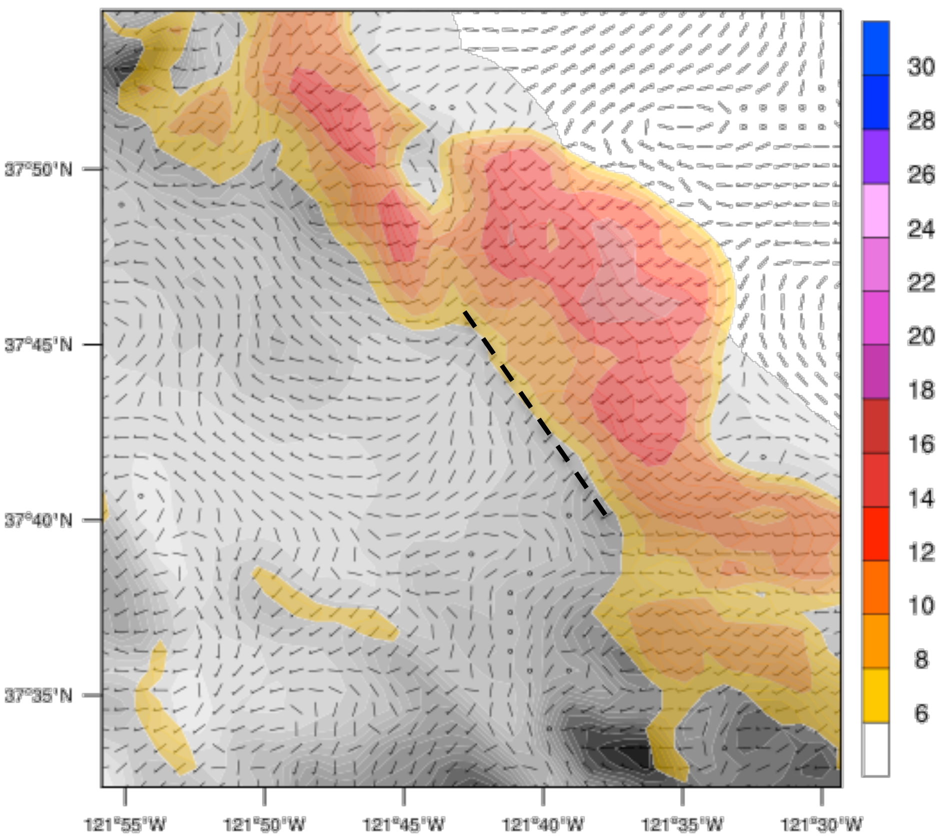

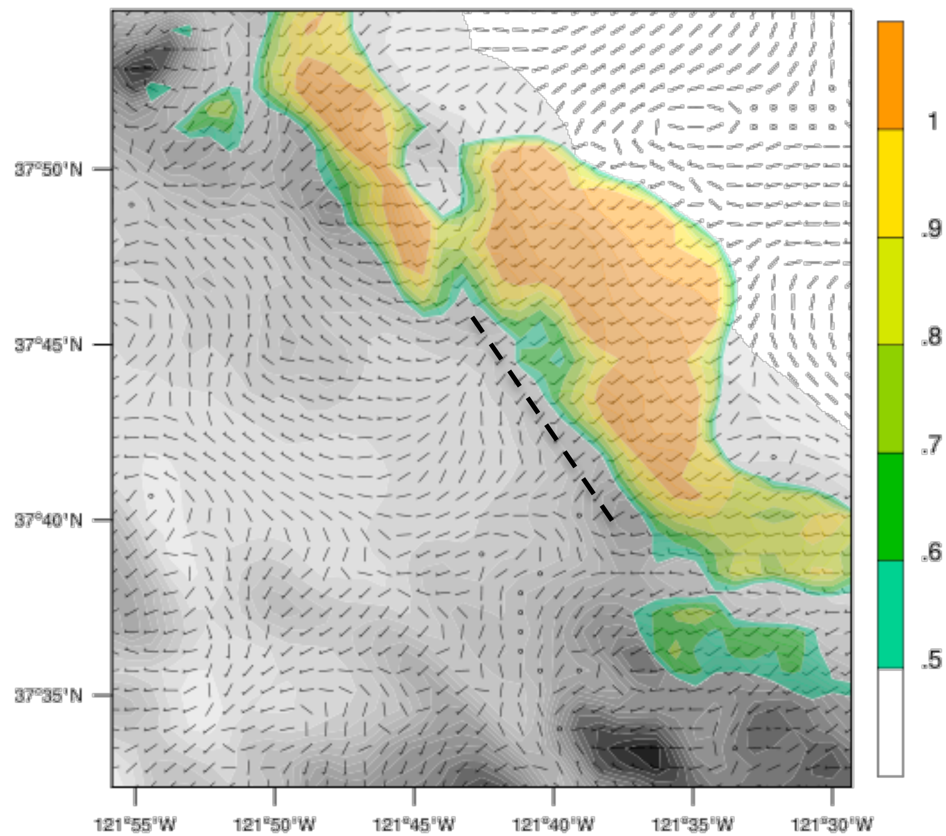

Elevation contoured every 100 m starting at 0 m AMSL (white). (a) Hub-height equivalent winds. Wind barbs, 10 m s^{-1}; half barb, 5 m s^{-1}. Winds $\geq$ 6 m s^{-1} are shaded in increments of 2 m s^{-1}. (b) Hub-height CF. CFs $\geq$ 0.5 are shaded in increments of 0.1. Dashed line marks location of Altamont Pass western ridgeline crest.

c. Wind Power Modeling July 25 1200 UTC (7/25 05 LT)

Winds and CF continue to decrease

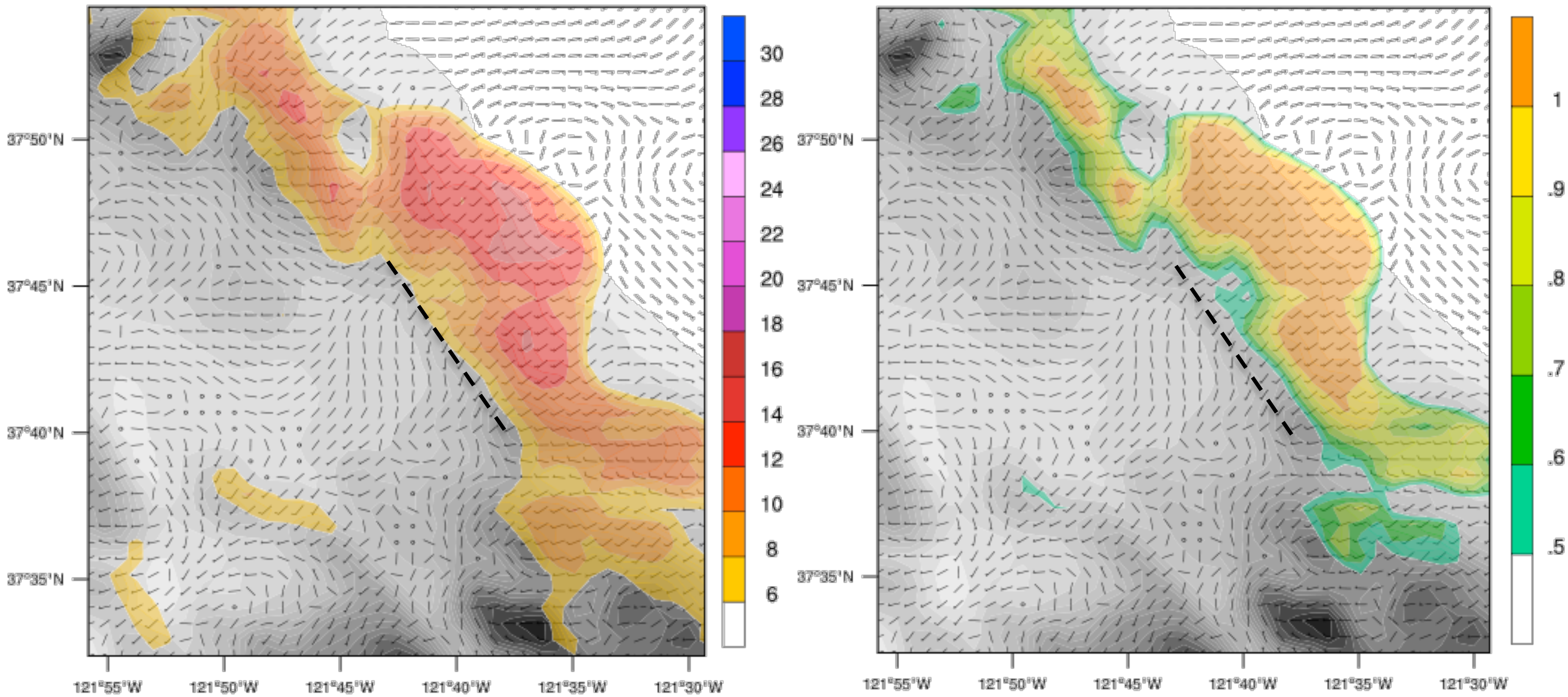

Elevation contoured every 100 m starting at 0 m AMSL (white). (a) Hub-height equivalent winds. Wind barbs, 10 m s^{-1}; half barb, 5 m s^{-1}. Winds $\geq$ 6 m s^{-1} are shaded in increments of 2 m s^{-1}. (b) Hub-height CF. CFs $\geq$ 0.5 are shaded in increments of 0.1. Dashed line marks location of Altamont Pass western ridgeline crest.

c. Wind Power Modeling July 25 1500 UTC (7/25 08 LT)

Winds and CF continue to decrease

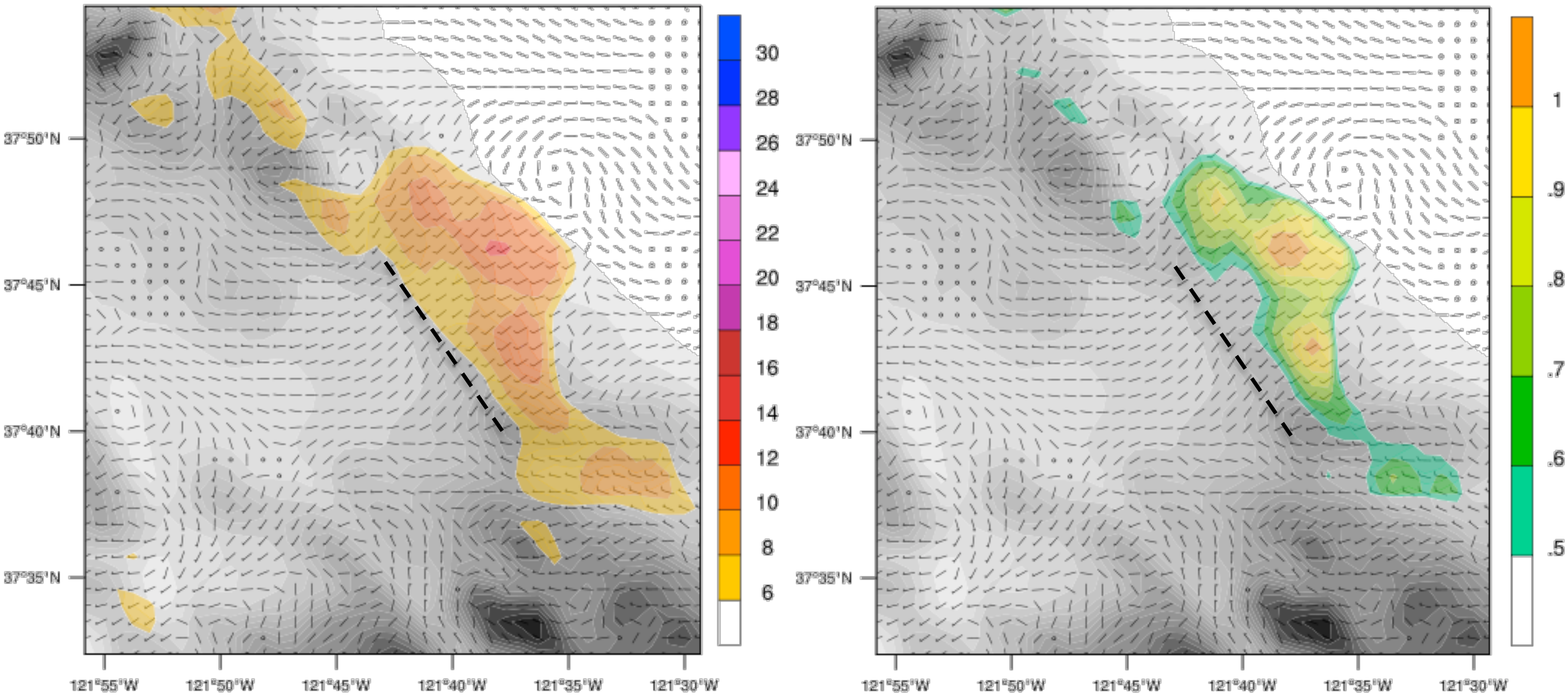

Elevation contoured every 100 m starting at 0 m AMSL (white). (a) Hub-height equivalent winds. Wind barbs, 10 m s^{-1}; half barb, 5 m s^{-1}. Winds $\geq$ 6 m s^{-1} are shaded in increments of 2 m s^{-1}. (b) Hub-height CF. CFs $\geq$ 0.5 are shaded in increments of 0.1. Dashed line marks location of Altamont Pass western ridgeline crest.

c. Wind Power Modeling July 25 1800 UTC (7/25 11 LT)

Winds are once again light…low CF

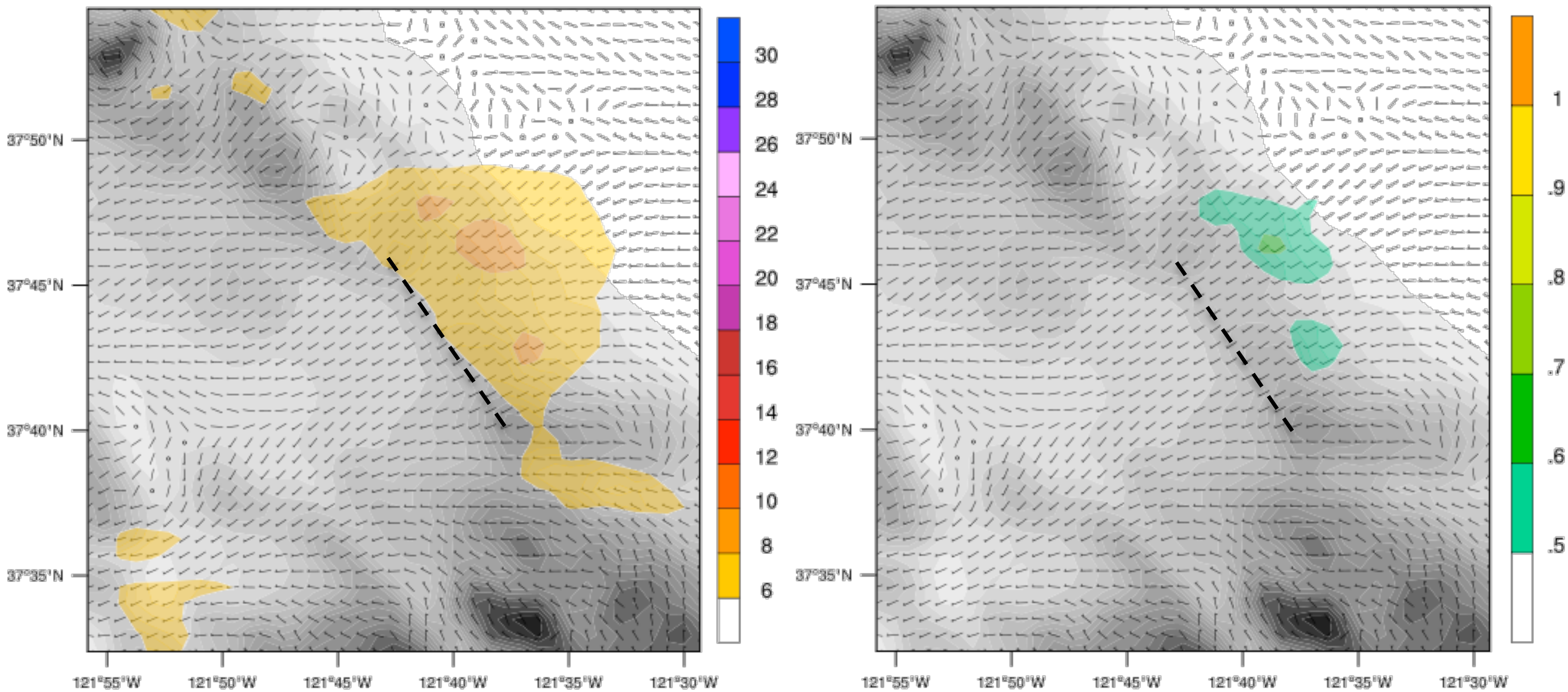

Elevation contoured every 100 m starting at 0 m AMSL (white). (a) Hub-height equivalent winds. Wind barbs, 10 m s^{-1}; half barb, 5 m s^{-1}. Winds $\geq$ 6 m s^{-1} are shaded in increments of 2 m s^{-1}. (b) Hub-height CF. CFs $\geq$ 0.5 are shaded in increments of 0.1. Dashed line marks location of Altamont Pass western ridgeline crest.

c. Wind Power Modeling: Summary

- WRF model results show Altamont Pass
  - With CF of 0.5 or greater for 16 hours of a LSMF day
  - With near optimal CF for at least 6 hours during the late afternoon into evening
- Wind directions through Altamont Pass remain relatively constant
  - NW to W upwind
  - WSW through Pass
  - W to NW downwind
- Matches findings of Zangl (2003) and Gabersek and Durran (2004)

Wind Power Modeling: Performance

- The hourly ***wind power*** was summed for 24 hour periods to determine **modeled daily CF**
- Compared to area turbine observations provided by an Altamont Pass wind power company

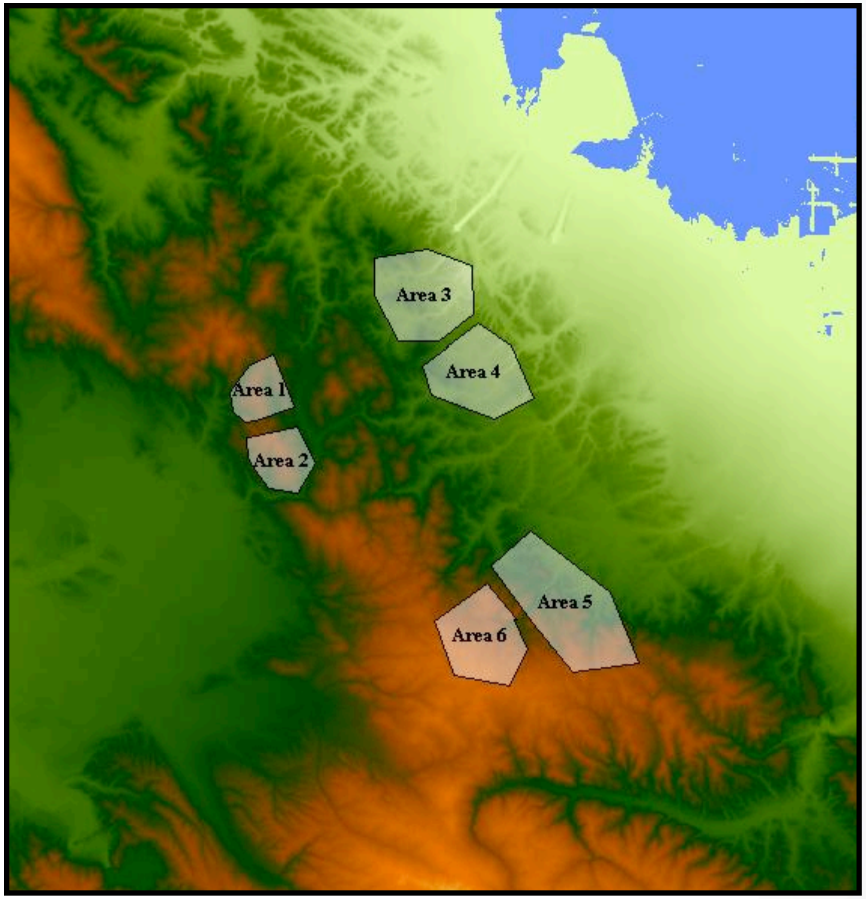

d. Wind Power Modeling Performance

Comparing modeled to observed daily CF:

All Areas

Time Period	Within Obs. Range	Within 1σ of Obs Area Avg.	Over-Predicted	Under-Predicted
Day 1	100%	66%	17%	17%
Day 2	90%	53%	30%	17%
Day 3	90%	36%	47%	17%

Excluding Areas 1 and 2

Time Period	Within Obs. Range	Within 1σ of Obs Area Avg.	Over-Predicted	Under-Predicted
Day 1	100%	**75%**	**25%**	**0%**
Day 2	**95%**	**55%**	**45%**	**0%**
Day 3	90%	**25%**	**75%**	**0%**

Excluding Areas 1 and 3

Time Period	Within Obs. Range	Within 1σ of Obs Area Avg.	Over-Predicted	Under-Predicted
Day 1	100%	**90%**	**10%**	**0%**
Day 2	**95%**	**75%**	**25%**	**0%**
Day 3	90%	**50%**	**50%**	**0%**

Improved **Worsened**

d. Wind Power Modeling Performance

- Modeled daily CF was outside the range of observed daily CF values in only 6 out of 90 instances!

- Interpolation sites within each area may be better at representing the high/low end of power production spectrum

Summary and Conclusions: Goals Revisited

During LSMF synoptic conditions:

1. Simulate the near-surface winds in Coast Ranges
2. Simulate winds and wind power in Altamont Pass
3. Assess the accuracy and potential of WRF as a wind power forecasting tool.

Summary and Conclusions: Findings

Simulation	WRF Model Performance
Coast Range Near-Surface Winds	Good
Altamont Pass Low-Level Winds	Acceptable to Good
Altamont Pass Wind Power	Good

- While modeled hour-to-hour variance was not exact, WRF-modeled wind speeds were close to those observed.
- Combined with good agreement between modeled and observed wind directions and atmospheric stability, **modeled daily capacity factors** were within the range of **observed daily capacity factors** in 93% percent of instances
- **WRF can be used as a wind power forecasting tool for Altamont Pass and possibly other coastal complex terrain regions.**

Summary and Conclusions

- Sources of Error
  - Errors fed in by NAM 218 boundary conditions
  - Internal model chaos
  - Interpolation sites
- Future Work
  - More case studies
  - Adjust for model biases
  - Gradient forecasting

Acknowledgements

- Dr. Craig Clements
- Dr. Alison Bridger
- Dr. Martin Leach
- Dr. Sharon Zhong
- Mike Voss
- Estatio Gutierrez
- All SJSU Meteorology Grads
- The Whole SJSU Meteorology Dept
- My Parents
- Briana

References

- Archer, C. L., M. Z. Jacobson, 2005: The Santa Cruz Eddy. Part II: Mechanisms of Formation. *Mon. Wea. Rev.,* **133**, 2387-2405. Doi: 10.1175/MWR2979.1
- Barry, R. G. 1992: *Mountain Weather and Climate.* 2nd ed. Routledge, 402 pp.
- Bathurst, G. N., J. Weatherill, and G. Strbac, 2002: Trading Wind Generation in Short Term Energy Markets. *Power Systems, IEEE Transactions on,* **17**, 782-789.
- Brown, B. G., R. W. Katz, and A. H. Murphy, 1984: Time Series Models to Simulate and Forecast Wind Speed and Wind Power. *Jour. of App. Met.,* **23,** 1184-1195.
- Burk, S. D., W. T. Thompson, 1996: The Summertime Low-Level Jet and Marine Boundary Layer Structure along the California Coast. *Mon. Wea. Rev.*, **124**, 668–686.
- Doran, J. C. and S. Zhong, 2000: Thermally Driven Gap Winds into the Mexico City Basin. *Jour. of App. Met.,* **39,** 1330-1340.
- Doyle, J. D. and R. B. Smith, 2003: Mountain waves over the Hohe Tauern: Influence of Upstream Diabatic Effects. *Q. J. R. Meteorol. Soc.*, **129,** 799-823, doi:10.1256
- Fosberg, M. A. and M. J. Schroeder, 1966: Marine Air Penetration in Central California. *Jour. Of App. Met.,* **5,** 573-589.
- Gaberšek, Saša, Dale R. Durran, 2004: Gap Flows through Idealized Topography. Part I: Forcing by Large-Scale Winds in the Non-rotating Limit. *J. Atmos. Sci.*, **61**, 2846–2862.
- Gaberšek, Saša, Dale R. Durran, 2006: Gap Flows through Idealized Topography. Part II: Effects of Rotation and Surface Friction. *J. Atmos. Sci.*, **63**, 2720–2739.
- Gazzilli, G., S. Palmieri, A. M. Siani, and G. R. Casale, 2001: In search of Mountain Sites Suitable for Wind Farms in the Mediterranean Area using a Diagnostic Wind Model. *Meteorol. Appl.,* **8,** 205-208.
- Jaramillo, O. A., and M. A. Borja, 2004: Wind Speed Analysis in La Ventosa, Mexico: a Bimodal Probability Distribution Case. *Renewable Energy,* **29,** 1613-1630.
- Jiménez, P. A., E. García-Bustamante, J. F. González-Rouco, J. Navarro, J. P. Montávez, J. V. G. de Arellano, J. Dudhia, and A. Muñoz-Roldan, 2010: Surface Wind Regionalization over Complex Terrain: Evaluation and Analysis of a High-Resolution WRF Simulation. *Jour. of App. Met. and Clim.,* **49**, 268-287.

References

- Kariniotakis, G., P. Pinson, N. Siebert, G. Giebel, and R. Barthelmie, 2004: The State of the Art in Short- Term Prediction of Wind Power-from an Offshore Perspective. *IEEE*, 20-21.
- Reid, S. J., R. Turner, 2001: Correlation of Real and Model Wind Speeds in Different Terrains. *Weather and Forecasting,* **16**, 620-627.
- Rife, D. L., C. A. Davis, Y. Liu, and T. T. Warner, 2004: Predictability of Low-Level Winds by Mesoscale Meteorological Models. *Mon. Weather Rev.,* **132**, 2553-2569.
- Sharp, J., and C. F. Mass, 2004: Columbia Gorge Gap Winds: Their Climatological Influence and Synoptic Evolution. Thesis, Dept. of Atmospheric Sciences, University of Washington, 56 pp.
- Skamarock, W. C., J. B. Klemp, J. Dudhia, D. O. Gill, D.M. Barker, W. Wang, and J. G. Powers, 2008: A Description of the Advanced Research WRF Version 3. NCAR Tech. Note TN-475+STR. 125 pp.
- Wagner, R., I. Antoniou, S. M. Pedersen, M. S. Courtney, and H. E. Jørgensen, 2009: The Influence of the Wind Speed Profile on Wind Turbine Performance Measurements. *Wind Energy,* **12**, 348-362.
- Wharton, S., J. Lundquist, 2010: Atmospheric Stability Impacts on Power Curves of Tall Wind Turbines — An Analysis of a West Coast North American Wind Farm. Technical report, Lawrence Livermore National Laboratory (LLNL), LLNL-TR-424425, 73 pp.
- Whiteman, C. D., 2000: *Mountain Meteorology: Fundamentals and Applications*. Oxford UP,
- Wiser, R., and M. Bolinger, 2008: Annual Report on U.S. Wind Power Installation, Cost and Performance Trends: 2007. U.S. DOE Publication DOE/GO-102008-2590.
- Žagar, N., M. Žagar, J. Cedilnik, G. Gregorič, and J. Rakovec, 2006: Validation of Mesoscale Low-Level Winds Obtained by Dynamical Downscaling of ERA40 over Complex Terrain. *Tellus A,* **58**, 445-455.
- Zangl, G., 2003: Orographic Gravity Waves Close to the Nonhydrostratic Limit of Vertical Propagation. *Jour. of Atmos. Sci.,* **60,** 2045-2063.
- Zaremba, L. L., and J. J. Carroll, 1999: Summer Wind Flow Regimes over the Sacramento Valley. *Jour. Of App. Met.,* **38,** 1463-1473.

Questions?